Accurate Identification of Bioactive Meliaceae Limonoids by UHPLC−MS/MS Based Structure−Fragment Relationships (SFRs)

Fayaj A. Mulani, Sharvani S. Nandikol,[#] Saikat Haldar,[#] and Hirekodathakallu V. Thulasiram*

Read Online

ACCESS | Metrics & More | Article Recommendations | SI Supporting Information

ABSTRACT: Limonoids are bioactive plant specialized metabolites found in the Meliaceae family. The basic limonoids, i.e., azadiradione, epoxyazadiradione, and gedunin have been exploited for various bioactivities and therefore are the potential drug leads for tomorrow. However, their low abundance, structural similarity, and lack of adequate mass fragmentation data have hampered their accurate identification and quantification from various sources. In the present study, basic limonoids such as azadirone, azadiradione, epoxyazadiradione, and gedunin isolated from Neem were utilized for the synthesis of their derivatives and isotopologs. A total of 30 one compounds were used in this study among which five were isolated, two were biotransformed, and 24 were synthesized. Among the synthesized compounds nine are novel compounds including six deuterated analogs/isotopologs which are (1,3-²H)-1,2-dihydro-3β-hydroxyazadiradione (**9**), (1,3,16-²H)-1,2-dihydro-3β-16β-dihydroxyazadir-adione (**10**), 3β-hydroxyazadiradione (**11**), 3β-16β-dihydroxyazadiradione (**12**), (3-²H)-3β-hydroxyazadiradione (**13**), (3,16-²H)-3β-16β-dihydroxyazadiradione (**14**), (1,3,7-²H)-1,2-dihydro-3β-hydroxy-7-deace-tylazadiradione (**15**), 1,2,20,21,22,23-hexahydroazadiradione (**17**), and (1,3-²H)-1,2-dihydro-3β-hydroxygedunin (**29**). These limonoids along with their semisynthesized derivatives were subjected to ultra high performance liquid chromatography mass spectrometry (UHPLC−MS/MS) and the fragmentation pathway was established based on structure−fragment relationships (SFRs), utilizing high resolution MS/MS data. We have developed a most reliable and easily reproducible protocol describing in depth analysis of SFRs based on the structural modifications and synthesis of isotopologs. Also, the MS/MS fragment library of these basic limonoids generated in this study acts as a fingerprint for accurate identification and quantification of limonoids by MS/MS analysis in various plant tissue extracts, phytopharmaceutical formulations and biological samples.
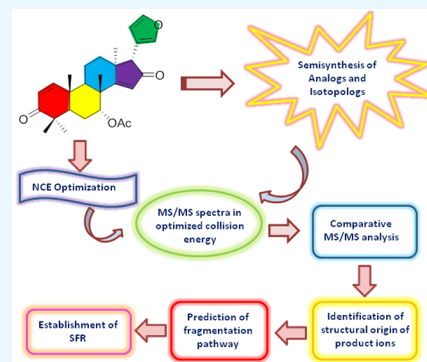
1. INTRODUCTION

In recent years, tandem mass spectrometry (MS) has over-shadowed the other analytical techniques for the structural prediction of individual components in low quantity complex mixture of organic small-molecules especially natural products.[1−11] Usual approaches for the identification of an analyte through mass spectrometry includes (i) coanalysis with the reference sample, (ii) comparison to the experimental reference data obtained from mass spectral libraries or predicted *in silico* mass spectra, and (iii) generation of empirical formula supporting the mass fragments and establishment of their structure−fragment relationships.[4,7] Unavailability of the reference compound or mass-repository data often compels the analytical chemists to adopt the third and last approach for the structure prediction.

The fragment/product ions[11] generated through tandem mass spectrometry can be assigned individually to their tentative chemical structures by deriving the fragmentation pathway, which is termed as the "structure−fragment relationship" or "structure−product ion relationship" (SFR). The SFR of a known molecule can be utilized for predicting the SFRs of unknown molecules, if the structure of an unknown analyte is a derivative or analog to the known precursor molecule. It has

been utilized widely as a routine technique for the rapid screening of natural sources in search of novel members of a predefined skeleton,[2,12−16] studying the metabolism of pharmaceuticals,[17−20] predicting the structure of unknowns in metabolomics,[3,21−23] differentiation of a region or stereo-isomeric compounds,[24−27] "dereplication" of natural products,[6,28] degradation studies,[29−33] and so on. For example, over two thousand articles have been published in the last ten years on the investigation of drug metabolism through mass spectrometry according to the information sourced from ISI Web of Science using the various combinations of keyword inputs such as "mass spectrometry", "MS", "drug", "metabo-lism", and "metabolite".

Identification of unknown volatiles/semivolatiles through the electron−ionization (EI) technique can be performed con-
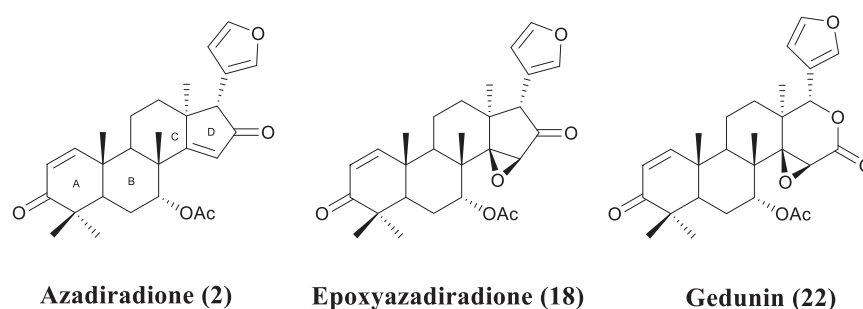
Figure 1. Structures of basic limonoids.

veniently due to the availability of large mass spectral libraries.[4,7] For example, the well-known NIST20 library (http://www.sisweb.com/software/ms/nist.htm) reserves 350,643 EI-MS spectra for 306,869 unique molecules. However, nonvolatile small molecules are ionized through soft-ionization techniques (such as ESI, MALDI, and APCI) and further analyzed by quadrupole, time-of-flight, ion trap, or hybrid technology. Moreover, they are subjected to tandem mass spectrometry for the fragmentation of molecular ion to generate product ions carrying valuable structural information. Unfortunately, the available count of the MS–MS spectra in mass repositories for nonvolatiles is truly insufficient considering their huge structural diversity. For instance, NIST20 holds MS/MS spectra of about 31,000 unique molecules in total. Consequently, SFRs often play a pivotal role for the structural elucidation of these molecules. To date, the interpretation of SFR is based on some empirical fragmentation rules (such as even-electron ion), preobserved regularities in fragmentation of a specific class of molecule, neutral loss/formation of stable ion isotopic distribution pattern, or comparison to algorithm based *in silico* fragmentation.[4,7,34] Especially, in the case of complex multifunctional organic molecules the prediction of SFR is more complicated due to the presence of several alternative routes for the generation of the same product ion.[35,36] Therefore, development of a technique which incorporates higher reliability in SFR prediction is greatly desirable because the authenticity of a predicted structure is highly dependent on the quality of proposed SFRs.

In this Article, a promising protocol has been described to bring deeper insight into SFRs based on the structural modification and synthesis of isotopologs (i.e., chemical species differing only in their isotopic composition) of the molecules of interest. Valuable information obtained on the structural origin of the fragments through simple semisynthesis of the derivatives greatly assists in predicting the SFRs of structurally complex molecules. Applicability of the protocol was further validated by predicting the SFRs (MS/MS) of basic limonoids, a class of tetranortriterpenoids,[37,38] viz., azadiradione (**2**), epoxyazadiradione (**18**), and gedunin (**22**) (Figure 1). In this manuscript we have developed a UHPLC–MS/MS based method for identification of structural fragments of basic limonoids. The tentative SFRs of product ions generated from the 28 analogs were deduced.

2. RESULTS AND DISCUSSION

The developed protocol for delineating reliable SFR of complex organic molecules is based on structural modifications and isotope labeling (isotopologs) of the precursor molecule. Functional groups (mostly oxygenated), ornamentally present on the skeleton of the organic framework are often responsible for the initiation of ionization in soft-ionization techniques.

Modifications of these moieties will potentially alter the fragmentation pathway leading to the variation in tandem mass fragments and their relative intensities. Therefore, variation in abundance (i.e., relative intensity) of individual product ions caused by specific structural modification states their "structural origin" and "fragmentation pathway" (i.e., "root" and route), aiding the establishment of SFRs. On the other hand, isotopologs usually follow the identical fragmentation pathway showing similar intensities for the mechanistically identical product ions, thus making the analysis easier and authentic. Tandem mass spectra of isotopologs clearly notify the presence/absence of labeling on each and every product ions. This is highly informative to decipher the "structural origin" and construct SFRs. The developed method was performed through a number of systematic steps as follows:

2.1. Structural Modifications and Semisynthesis of Isotopologs. Azadiradione (**2**), epoxyazadiradione (**18**), and gedunin (**22**) isolated from Neem were subjected to strategic synthetic protocols for structural modifications to construct a small library of structural analogs. Similarly, isotopologs were synthesized using isotope-labeled reagents. All the synthesized structurally different analogs of basic limonoids were characterized by NMR and used for MS/MS fragmentation studies.

2.1.1. Semisynthesis of Azadiradione (2) Derivatives. Semisynthesis of azadiradione (**2**) derivatives is illustrated in Scheme 1. Compound **3** was obtained by treating **2** with methanolic K_2CO_3, which on further oxidation using PCC gave **4**. Compounds **7**, **8** and **9**, **10** were obtained by the reduction of **2** with $NaBH_4$ and $NaBD_4$, respectively. $NaBD_4$ on reaction with **4** gave **15**. The Luche reduction of compound **2** with $NaBH_4 \cdot CeCl_3$ and $NaBD_4 \cdot CeCl_3$ yielded **11**, **12** and **13**, **14**, respectively. Compound **6** was obtained by epoxidation of **2**. Hydrogenation of compound **2** yielded **5**, **17**. The detailed description on synthesis of analogs is discussed in the Supporting Information (section A). Compounds **9–15**, **17** are novel and reported here for the first time.

2.1.2. Semisynthesis of Epoxyazadiradione (18) Derivatives. Epoxyazadiradione (**18**) was subjected to functional modification as shown in Scheme 2. Compound **19** was obtained by treating **18** with methanolic K_2CO_3, which on further oxidation with PCC yielded compound **20**. Hydrogenation of compound **18** by H_2/Pd generated compound **21**. The detailed description on synthesis of analogs is discussed in the Supporting Information (section A).

2.1.3. Semisynthesis of Gedunin (22) Derivatives. Functional modification of gedunin (**22**) is shown in Scheme 3. By deacetylation of **22** with saturated methanolic K_2CO_3 solution, compound **23** was synthesized. Reaction of **23** with H_2O_2, NaOH yielded compound **27** and with PCC yielded **24**, respectively. Hydrogenation of compound **22** generated

Scheme 1. Synthesis of Azadiradione (2) Derivatives[a]
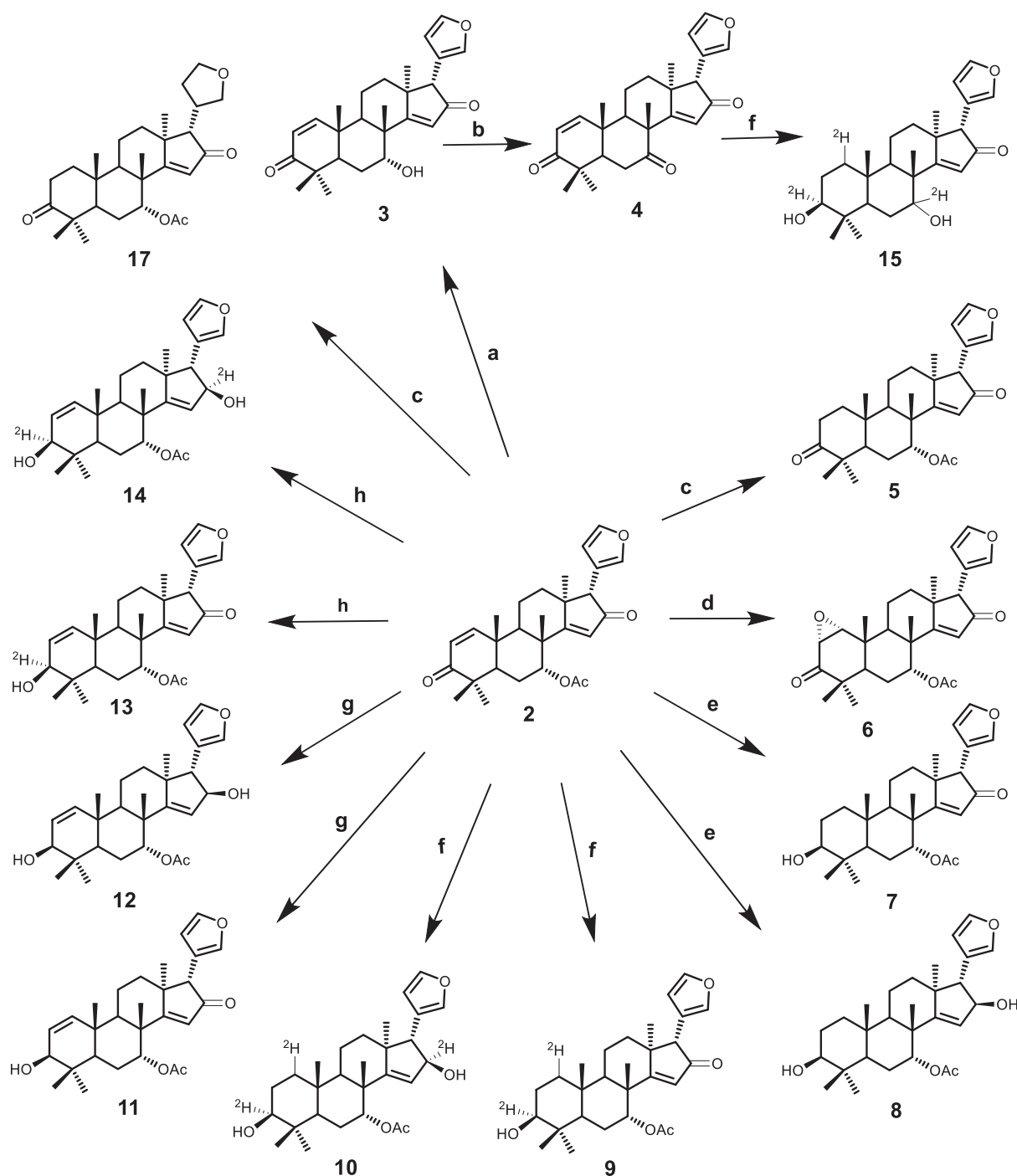
[a]Reagents and conditions: (a) K₂CO₃/MeOH, (b) PCC, (c) H₂/Pd, (d) H₂O₂/NaOH, (e) NaBH₄, (f) NaBD₄, (g) NaBH₄/CeCl₃, (h) NaBD₄/CeCl₃.

compound **25** and epoxidation of compound **22** in the presence of H₂O₂, NaOH gave **26**. The treatment of **22** with NaBH₄ and NaBD₄ individually gave compounds **28** and **29**, respectively. The detailed description on synthesis of analogs is discussed in the Supporting Information (section A). Among the synthesized derivatives of **22**, compound **29** is novel with deuteration at C1 and C3.

2.2. Optimization of Collision Energy. The abundance of product ions in tandem mass spectroscopy is highly dependent on the intensity of collision energy employed. More energy

enhances the intensity of low mass fragments and vice versa. Therefore, collision energy was optimized to achieve significant abundance of product ions in tandem mass spectra of precursor molecules throughout an energy range. MS/MS analysis was investigated by employing high-energy C-trap dissociation (HCD) with orbitrap detection.

The limonoids azadiradione (**2**), epoxyazadiradione (**18**), and gedunin (**22**) were used as representatives for the optimization study with variable normalized collision energy (NCE) of 15, 20, 25, 30, and 35%; this was plotted as variation in

**Scheme 2. Synthesis of Epoxyazadiradione (18) Derivatives**[a]
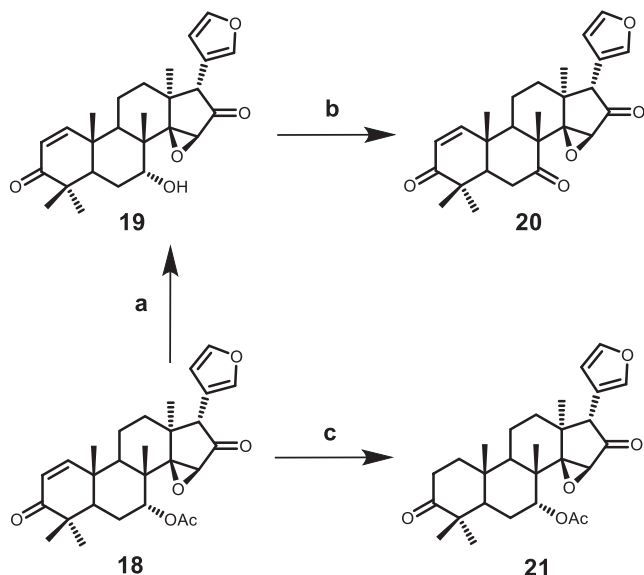
[a]Reagents and conditions: (a) K$_2$CO$_3$/MeOH, (b) PCC, (c) H$_2$/Pd.

intensities of the fragments with that of sweeping collision energy (Figure 2). The NCE of 25% was established to generate the product ions of both high and low mass fragments throughout. This was favored for all basic limonoids and their derivatives.

2.3. Recording of Tandem Mass Spectra. By applying the optimized collision energy, MS/MS spectra were recorded for the molecular ion in all structural analogs. The precursor ion and their product ions with corresponding chemical formula and percent intensity are well documented as shown in Tables 1, 2, and 3.

2.4. Tentative Structural Identification of the Product Ions. As mentioned above, modification(s) of skeletal functional groups may not only change the list of tandem mass fragments but also their abundances. Extinction/lowering of intensity of specific product ions is due to the modification on a distinct structural part indicating the origin of product ions. This probability was evaluated through different modifications on the same structural part and the effect on the product ion was analyzed. Higher confidence was gained over the prediction by analyzing the tandem mass spectra of corresponding isotopolog.

2.5. Elucidating the MS/MS Fragmentation Pathway of the Precursor Ions and Establishing SFRs. Knowing the

Scheme 3. Synthesis of Gedunin (22) Derivatives[a]
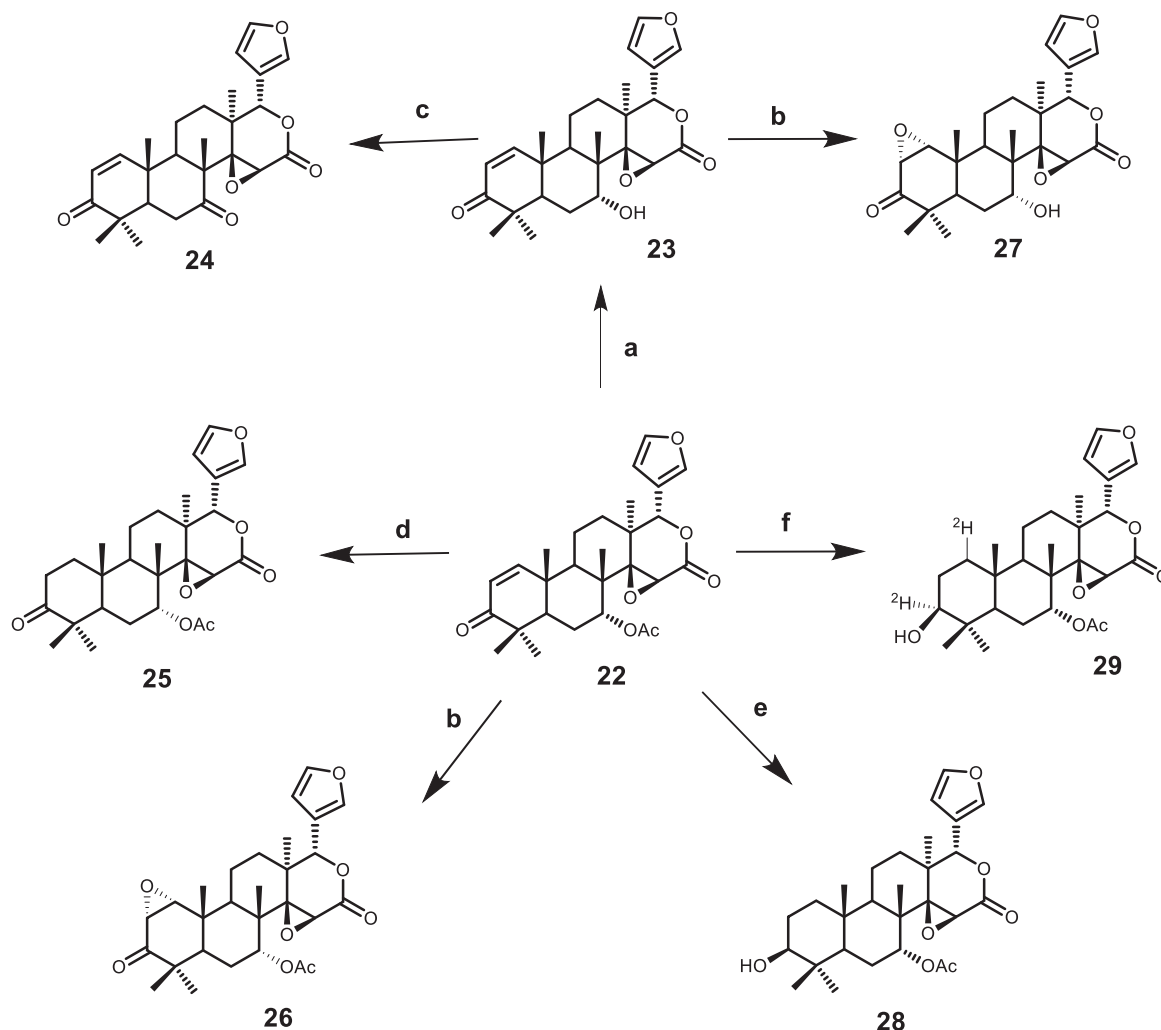
[a]Reagents and conditions: (a) K$_2$CO$_3$/MeOH, (b) H$_2$O$_2$/NaOH, (c) PCC, (d) H$_2$/Pd, (e) NaBH$_4$, (f) NaBD$_4$.
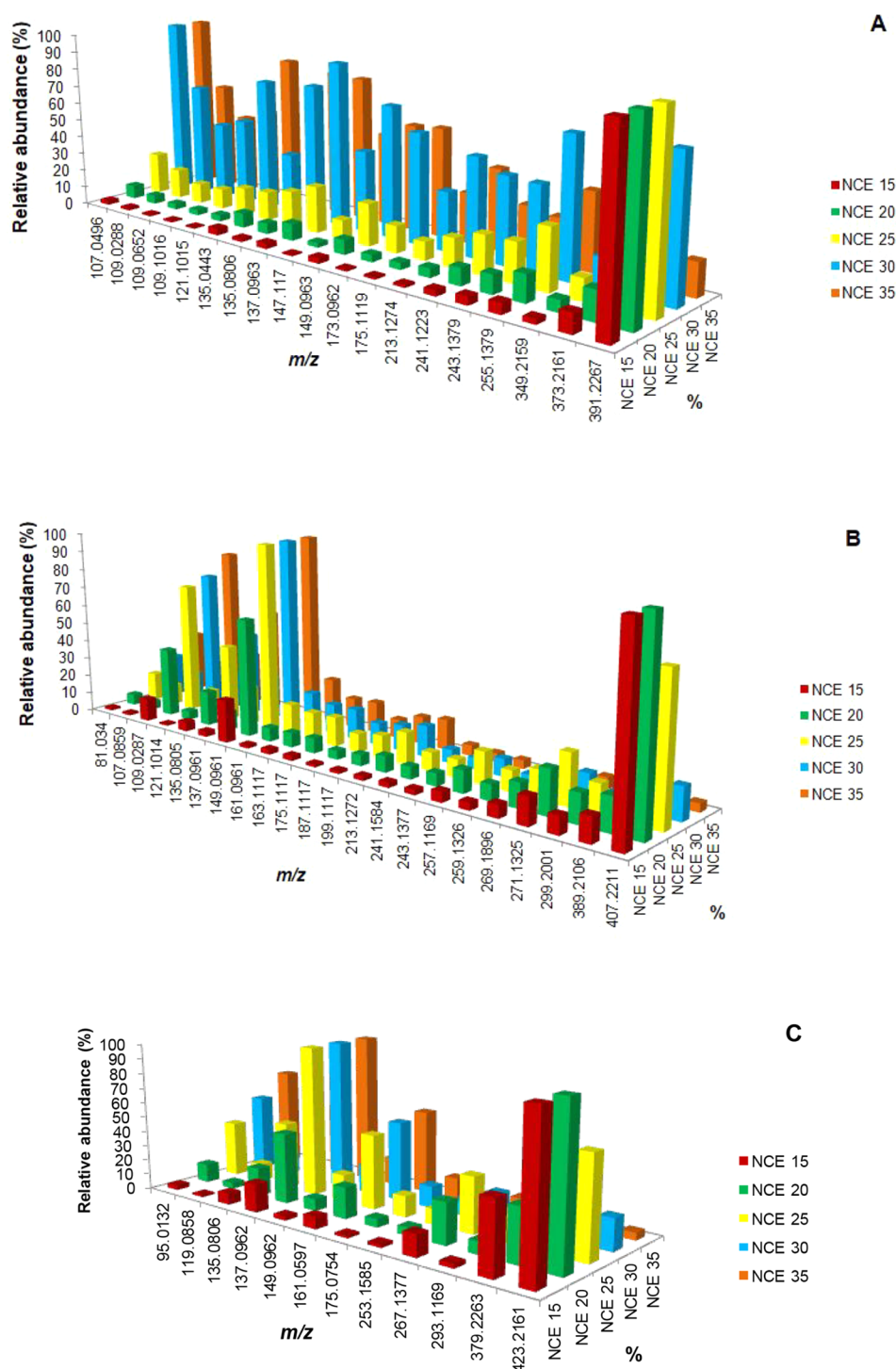
Figure 2. Variation in relative intensity of MS/MS product ions with varying NCE for (A) azadiradione (**2**), (B) epoxyazadiradione (**18**), and (C) gedunin (**22**).

structural origin of product ions, the fragmentation pathway was elucidated manually with higher confidence for compounds **2**, **18**, and **22** and their respective derivatives. SFRs of product ions were established with high accuracy (error <5 ppm) by comparative HCD-MS/MS analyses of the 17 precursor ions for **2**, four precursor ions for **18**, and ten precursor ions for **22**. The information generated on SFRs will guide the structural elucidation of unknown analog by comparative analysis. The complete protocol for elucidation of SFRs is represented in

Figure 3. The following section discusses fragmentation pathways and SFRs in detail based on MS/MS characterization.

2.5.1. MS/MS Characterization of Azadiradione (2) and Its Derivatives. The tentative fragmentation pattern was obtained by subjecting azadiradione (**2**) and its derivatives to the HCD-MS/MS studies with 25% NCE (Table 1) and are schematically represented in Figures 4, 5, 6, and S174. Functionally modified derivatives of azadiradione (**2**), viz., **3** (7-deacetylazadiradione), **4** (7-oxoazadiradione), **5** (1,2-dihydroazadiradione), **6** (1,2α-

Table 1. Structure, Precursor Ion, and Their Product Ions (with Corresponding Chemical Formula and % Intensity) of Azadiradione (2) and Its Derivatives

No.	Structure	Precursor ion (m/z)	Product ions m/z (formula, % intensity at NCE 25 %)
1		[M+H]$^+$ 437.2687	95.0495 (C_6H_7O, 43.86), 107.0495 (C_7H_7O, 12.42), 109.0651 (C_7H_9O, 18.12), 109.1014 (C_8H_{13}, 21.74), 121.1013 (C_9H_{13}, 24.36), 121.0650 (C_8H_9O, 19.47), 135.0805 ($C_9H_{11}O$, 26.01), 137.0961 ($C_9H_{13}O$, 31.17), 147.1168 ($C_{11}H_{15}$, 26.0), 149.0960 ($C_{10}H_{13}O$, 84.66), 175.1116 ($C_{12}H_{15}O$, 35.76), 213.1272 ($C_{15}H_{17}O$, 23.62), 215.1428 ($C_{15}H_{19}O$, 62.12), 227.1427 ($C_{16}H_{19}O$, 49.24), 229.1584 ($C_{16}H_{21}O$, 18.15), 241.1584 ($C_{17}H_{21}O$, 30.54), 377.2468 ($C_{26}H_{33}O_2$, 100.0).
2		[M+H]$^+$ 451.2483	107.0496 (C_7H_7O, 22.98), 109.0288 ($C_6H_5O_2$, 16.40), 109.0652 (C_7H_9O, 11.05), 109.1016 (C_8H_{13}, 11.13), 121.1015 (C_9H_{13}, 14.98), 135.0443 ($C_8H_7O_2$, 16.02), 135.0806 ($C_9H_{11}O$, 19.72), 137.0963 ($C_9H_{13}O$, 25.80), 147.1170 ($C_{11}H_{15}$, 10.61), 149.0963 ($C_{10}H_{13}O$, 23.37), 173.0962 ($C_{12}H_{13}O$, 14.90), 175.1119 ($C_{12}H_{15}O$, 10.17), 213.1274 ($C_{15}H_{17}O$, 15.98), 241.1223 ($C_{16}H_{17}O_2$, 21.46), 243.1379 ($C_{16}H_{19}O_2$, 21.78), 255.1379 ($C_{17}H_{19}O_2$, 33.24), 349.2159 ($C_{24}H_{29}O_2$, 11.84), 373.2161 ($C_{26}H_{29}O_2$, 19.17), 391.2267 ($C_{26}H_{31}O_3$, 100).
3		[M+H]$^+$ 409.2377	107.0495 (C_7H_7O, 3.56), 109.0288 ($C_6H_5O_2$, 5.46), 109.0651 (C_7H_9O, 2.21), 109.1015 (C_8H_{13}, 1.58), 121.1014 (C_9H_{13}, 2.57), 135.0442 ($C_8H_7O_2$, 1.92), 135.0806 ($C_9H_{11}O$, 13.82), 137.0962 ($C_9H_{13}O$, 4.19), 147.1169 ($C_{11}H_{15}$, 1.18), 149.0962 ($C_{10}H_{13}O$, 7.44), 173.0962 ($C_{12}H_{13}O$, 6.20), 175.1118 ($C_{12}H_{15}O$, 4.15), 213.1274 ($C_{15}H_{17}O$, 4.37), 241.1222 ($C_{16}H_{17}O_2$, 4.52), 243.1378 ($C_{16}H_{19}O_2$, 1.69), 255.1378 ($C_{17}H_{19}O_2$, 4.76), 305.1895 ($C_{22}H_{25}O$, 0.71), 373.2158 ($C_{26}H_{29}O_2$, 5.39), 391.2264 ($C_{26}H_{31}O_3$, 25.67).
4		[M+H]$^+$ 407.2211	107.0494 (C_7H_7O, 25.10), 109.0287 ($C_6H_5O_2$, 19.24), 109.0651 (C_7H_9O, 3.84), 109.1014 (C_8H_{13}, 3.39), 121.1013 (C_9H_{13}, 4.14), 135.0441 ($C_8H_7O_2$, 7.29), 135.0805 ($C_9H_{11}O$, 33.71), 137.0961 ($C_9H_{13}O$, 11.16), 147.1168 ($C_{11}H_{15}$, 3.86), 149.0961 ($C_{10}H_{13}O$, 13.14), 173.0961 ($C_{12}H_{13}O$, 8.81), 175.1115 ($C_{12}H_{15}O$, 22.06), 213.1273 ($C_{15}H_{17}O$, 8.53), 241.1220 ($C_{16}H_{17}O_2$, 2.32), 243.1377 ($C_{16}H_{19}O_2$, 1.81), 253.1220 ($C_{17}H_{17}O_2$, 6.50), 321.1845 ($C_{22}H_{25}O_2$, 1.91), 389.2106 ($C_{26}H_{29}O_3$, 10.29), 407.2213 ($C_{26}H_{31}O_4$, 100).
5		[M+H]$^+$ 453.2643	107.0494 (C_7H_7O, 15.52), 109.0287 ($C_6H_5O_2$, 20.47), 109.0650 (C_7H_9O, 2.06), 109.1014 (C_8H_{13}, 7.01), 121.1013 (C_9H_{13}, 3.57), 135.0441 ($C_8H_7O_2$, 11.80), 135.0805 ($C_9H_{11}O$, 1.63), 137.0960 ($C_9H_{13}O$, 5.18), 139.1117 ($C_9H_{15}O$, 3.62), 147.1167 ($C_{11}H_{15}$, 8.84), 151.1116 ($C_{10}H_{15}O$, 2.97), 173.0960 ($C_{12}H_{13}O$, 8.69), 175.1116 ($C_{12}H_{15}O$, 3.42), 177.1272 ($C_{12}H_{17}O$, 3.83), 213.1271($C_{15}H_{17}O$, 21.18), 215.1428 ($C_{15}H_{19}O$, 3.55), 241.1220 ($C_{16}H_{17}O_2$, 26.35), 243.1376 ($C_{16}H_{19}O_2$, 32.09), 255.1375 ($C_{17}H_{19}O_2$, 9.44), 349.2152 ($C_{24}H_{29}O_2$, 1.21), 375.2311 ($C_{26}H_{31}O_2$, 25.40), 393.2416 ($C_{26}H_{33}O_3$, 100).
6		[M+H]$^+$ 467.2430	107.0495 (C_7H_7O, 27.07), 109.0287 ($C_6H_5O_2$, 17.85), 109.0651 (C_7H_9O, 4.52), 109.1015 (C_8H_{13}, 2.89), 121.1014 (C_9H_{13}, 3.43), 135.0441 ($C_8H_7O_2$, 18.41), 135.0804 ($C_9H_{11}O$, 3.13), 137.0961 ($C_9H_{13}O$, 5.51), 147.1168 ($C_{11}H_{15}$, 3.99), 149.0961 ($C_{10}H_{13}O$, 2.59), 173.0960 ($C_{12}H_{13}O$, 10.65), 175.1117 ($C_{12}H_{15}O$, 2.80), 213.1272 ($C_{15}H_{17}O$, 91.34), 241.1220 ($C_{16}H_{17}O_2$, 38.71), 243.1376 ($C_{16}H_{19}O_2$, 7.27), 255.1376 ($C_{17}H_{19}O_2$, 5.59), 349.2146 ($C_{24}H_{29}O_2$, 0.16), 389.2106 ($C_{26}H_{29}O_3$, 14.76), 407.2211 ($C_{26}H_{31}O_4$, 100).
7		[M+H]$^+$ 455.2775	107.0492 (C_7H_7O, 6.50), 109.0285 ($C_6H_5O_2$, 30.43), 109.0649 (C_7H_9O, 1.56), 109.1012 (C_8H_{13}, 24.89), 121.1011 (C_9H_{13}, 7.15), 123.1167 (C_9H_{15}, 15.38), 135.0438 ($C_8H_7O_2$, 7.37), 135.0801 ($C_9H_{11}O$, 1.30), 135.1166 ($C_{10}H_{15}$, 15.25), 139.1115 ($C_9H_{15}O$, 5.28), 147.1165 ($C_{11}H_{15}$, 9.06), 159.1165 ($C_{12}H_{15}$, 6.09), 161.1321 ($C_{12}H_{17}$, 6.91), 173.0957 ($C_{12}H_{13}O$, 6.66), 177.1268 ($C_{12}H_{17}O$, 0.62), 213.1268 ($C_{15}H_{17}O$, 10.58), 217.1581 ($C_{15}H_{21}O$, 0.53), 241.1216 ($C_{16}H_{17}O_2$, 25.91), 243.1371 ($C_{16}H_{19}O_2$, 47.16), 255.1371 ($C_{17}H_{19}O_2$, 17.82), 349.2180 ($C_{24}H_{29}O_2$, 0.76), 377.2460 ($C_{26}H_{33}O_2$, 55.94), 395.2565 ($C_{26}H_{35}O_3$, 100).
8		[M+Na]$^+$ 479.2764	95.0495 (C_6H_7O, 6.91), 107.0493 (C_7H_7O, 0.90), 109.0650 (C_7H_9O, 1.79), 109.1013 (C_8H_{13}, 6.25), 119.0492 (C_8H_7O, 0.13), 121.1012 (C_9H_{13}, 5.77), 123.1168 (C_9H_{15}, 3.75), 135.0804 ($C_9H_{11}O$, 1.12), 135.1167 ($C_{10}H_{15}$, 23.51), 139.1118 ($C_9H_{15}O$, 0.62), 147.1166 ($C_{11}H_{15}$, 3.36), 159.1166 ($C_{12}H_{15}$, 6.76), 161.1322 ($C_{12}H_{17}$, 7.60), 173.0959 ($C_{12}H_{13}O$, 20.83), 177.1272 ($C_{12}H_{17}O$, 0.66), 213.1270 ($C_{15}H_{17}O$, 3.40), 217.1585 ($C_{15}H_{21}O$, 1.21), 225.1270 ($C_{16}H_{17}O$, 37.19), 227.1426 ($C_{16}H_{19}O$, 14.55), 239.1426 ($C_{17}H_{19}O$, 11.10), 379.2624 ($C_{26}H_{35}O_2$, 100), 397.2727 ($C_{26}H_{37}O_3$, 1.52).
9		[M+H]$^+$ 457.2915	107.0496 (C_7H_7O, 6.79), 109.0288 ($C_6H_5O_2$, 24.13), 110.0714 ($C_7H_8{}^2HO$, 0.29), 110.1078 ($C_8H_{12}{}^2H$, 10.36), 123.1137 ($C_9H_{11}{}^2H_2$, 1.63), 125.1297 ($C_9H_{13}{}^2H_2$ 2.43), 135.0442 ($C_8H_7O_2$, 6.66), 135.0805 ($C_9H_{11}O$, 1.07), 137.1296 ($C_{10}H_{13}{}^2H_2$, 8.97), 141.1245 ($C_9H_{13}{}^2H_2O$, 1.82), 147.1171 ($C_{11}H_{15}$, 5.66), 161.1322 ($C_{12}H_{13}{}^2H_2$, 1.58), 163.1451 ($C_{12}H_{15}{}^2H_2$, 3.35), 173.0962 ($C_{12}H_{13}O$, 7.99), 178.1355 ($C_{12}H_{16}{}^2HO$, 0.37), 213.1274 ($C_{15}H_{17}O$, 12.42), 219.1714 ($C_{15}H_{19}{}^2H_2O$, 0.55), 241.1223 ($C_{16}H_{17}O_2$, 28.98), 243.1379 ($C_{16}H_{19}O_2$, 40.88), 255.1378 ($C_{17}H_{19}O_2$, 16.04), 350.2224 ($C_{24}H_{28}{}^2HO_2$, 0.30), 379.2597 ($C_{26}H_{31}{}^2H_2O_2$, 61.02), 397.2702 ($C_{26}H_{33}{}^2H_2O_3$, 100).
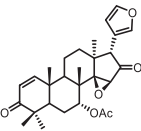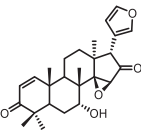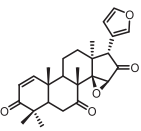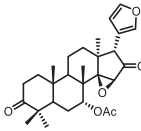
Table 1. continued

No.	Structure	Precursor ion (m/z)	Product ions m/z (formula, % intensity at NCE 25 %)
10		$[M+Na]^+$ 482.2944	96.0557 ($C_6H_6{}^2HO$, 2.41), 108.0556 ($C_7H_6{}^2HO$, 0.69), 110.0712 ($C_7H_8{}^2HO$, 0.97), 110.1076 ($C_8H_{12}{}^2H$, 3.69), 120.0554 ($C_8H_6{}^2HO$, 0.10), 123.1137 ($C_9H_{11}{}^2H_2$, 1.73), 125.1294 ($C_9H_{13}{}^2H_2$, 2.33), 135.0805 ($C_9H_{11}O$, 0.69), 137.1293 ($C_{10}H_{13}{}^2H_2$, 22.55), 141.1238 ($C_9H_{13}{}^2H_2O$, 0.13), 147.1134 ($C_{11}H_{15}$, 1.35), 161.1292 ($C_{12}H_{13}{}^2H_2$, 3.07), 163.1448 ($C_{12}H_{15}{}^2H_2$, 6.12), 174.1022 ($C_{12}H_{12}{}^2HO$, 17.94), 178.1333 ($C_{12}H_{16}{}^2HO$, 0.23), 214.1333 ($C_{15}H_{16}{}^2HO$, 2.72), 219.1710 ($C_{15}H_{19}{}^2H_2O$, 1.56), 226.1332 ($C_{16}H_{16}{}^2HO$, 38.23), 228.1489 ($C_{16}H_{18}{}^2HO$, 12.98), 240.1488 ($C_{17}H_{18}{}^2HO$, 10.43), 382.2809 ($C_{26}H_{32}{}^2H_3O_2$, 100), 400.2917 ($C_{26}H_{34}{}^2H_3O_3$, 1.34).
11		$[M+H]^+$ 453.2616	107.0493 (C_7H_7O, 10.69), 109.0285 ($C_6H_5O_2$, 20.89), 109.0649 (C_7H_9O, 3.27), 109.1013 (C_8H_{13}, 23.31), 121.1012 (C_9H_{13}, 14.15), 135.0439 ($C_8H_7O_2$, 9.89), 135.0802 ($C_9H_{11}O$, 3.86), 137.0959 ($C_9H_{13}O$, 6.92), 139.1116 ($C_9H_{15}O$, 1.66), 147.1166 ($C_{11}H_{15}$, 9.56), 151.1115 ($C_{10}H_{15}O$, 3.82), 173.0958 ($C_{12}H_{13}O$, 6.75), 175.1114 ($C_{12}H_{15}O$, 6.62), 177.1270 ($C_{12}H_{17}O$, 2.04), 213.1270 ($C_{15}H_{17}O$, 7.09), 215.1426 ($C_{15}H_{19}O$, 6.25), 241.1218 ($C_{16}H_{17}O_2$, 10.77), 243.1373 ($C_{16}H_{19}O_2$, 100), 255.1372 ($C_{17}H_{19}O_2$, 12.0), 349.2149 ($C_{24}H_{29}O_2$, 1.21), 375.2306 ($C_{26}H_{31}O_2$, 27.21), 393.2411 ($C_{26}H_{33}O_3$, 42.85).
12		$[M+Na]^+$ 477.2602	95.0495 (C_6H_7O, 25.96), 107.0494 (C_7H_7O, 6.47), 109.0650 (C_7H_9O, 7.93), 109.1013 (C_8H_{13}, 100), 119.0492 (C_8H_7O, 0.93), 121.1012 (C_9H_{13}, 23.03), 135.0803 ($C_9H_{11}O$, 9.41), 137.0959 ($C_9H_{13}O$, 16.05), 139.1116 ($C_9H_{15}O$, 0.69), 147.1166 ($C_{11}H_{15}$, 14.40), 151.1115 ($C_{10}H_{15}O$, 11.77), 173.0959 ($C_{12}H_{13}O$, 43.78), 175.1115 ($C_{12}H_{15}O$ 10.83), 177.1270 ($C_{12}H_{17}O$, 4.10), 213.1270 ($C_{15}H_{17}O$, 13.47), 215.1425 ($C_{15}H_{19}O$, 7.37), 225.1270 ($C_{16}H_{17}O$, 37.0), 227.1427 ($C_{16}H_{19}O$, 28.86), 239.1425 ($C_{17}H_{19}O$, 45.02), 349.2156 ($C_{24}H_{29}O_2$, 0.61), 377.2466 ($C_{26}H_{33}O_2$, 92.66), 395.2583 ($C_{26}H_{35}O_3$, 0.19).
13		$[M+H]^+$ 454.2679	107.0495 (C_7H_7O, 9.83), 109.0287 ($C_6H_5O_2$, 18.06), 109.0651 (C_7H_9O, 2.22), 109.1015 (C_8H_{13}, 5.25), 122.1077 ($C_9H_{12}{}^2H$, 11.88), 135.0441 ($C_8H_7O_2$, 7.99), 135.0804 ($C_9H_{11}O$, 2.28), 138.1024 ($C_9H_{12}{}^2HO$, 3.59), 140.1180 ($C_9H_{14}{}^2HO$, 1.36), 147.1168 ($C_{11}H_{15}O$, 9.14), 152.1180 ($C_{10}H_{14}{}^2HO$, 3.05), 173.0961 ($C_{12}H_{13}O$, 7.95), 176.1178 ($C_{12}H_{14}{}^2HO$, 3.87), 178.1337 ($C_{12}H_{16}{}^2HO$, 0.73), 213.1273 ($C_{15}H_{17}O$, 6.36), 216.1469 ($C_{15}H_{18}{}^2HO$, 1.93), 241.1222 ($C_{16}H_{17}O_2$, 9.33), 243.1377 ($C_{16}H_{19}O_2$, 100), 255.1377 ($C_{17}H_{19}O_2$, 10.55), 349.2119 ($C_{24}H_{29}O_2$, 0.09), 376.2376 ($C_{26}H_{30}{}^2HO_2$, 21.07), 394.2482 ($C_{26}H_{32}{}^2HO_3$, 24.74).
14		$[M+Na]^+$ 479.2717	96.0557 ($C_6H_6{}^2HO$, 3.82), 108.0555 ($C_7H_6{}^2HO$, 1.61), 109.0650 (C_7H_9O, 2.10), 109.1013 (C_8H_{13}, 4.80), 120.0555 ($C_8H_6{}^2HO$, 0.11), 122.1074 ($C_9H_{12}{}^2H$, 7.52), 135.0802 ($C_9H_{11}O$, 5.37), 138.1025 ($C_9H_{12}{}^2HO$, 2.24), 140.1178 ($C_9H_{14}{}^2HO$, 0.24), 147.1171 ($C_{11}H_{15}$, 1.77), 152.1177 ($C_{10}H_{14}{}^2HO$, 5.65), 174.1021 ($C_{12}H_{12}{}^2HO$, 11.29), 176.1177 ($C_{12}H_{14}{}^2HO$, 3.72), 178.1333 ($C_{12}H_{16}{}^2HO$, 1.43), 214.1331 ($C_{15}H_{16}{}^2HO$, 3.54), 216.1489 ($C_{15}H_{18}{}^2HO$, 2.27), 226.1331 ($C_{16}H_6{}^2HO$, 14.32), 228.1488 ($C_{16}H_{18}{}^2HO$, 6.24), 240.1486 ($C_{17}H_{18}{}^2HO$, 13.30), 350.2217 ($C_{24}H_{28}{}^2HO_2$, 0.56), 379.2585 ($C_{26}H_{31}{}^2H_2O_2$, 100), 397.2683 ($C_{26}H_{33}{}^2H_2O_3$, 0.20).
15		$[M+H]^+$ 416.2858	107.0492 (C_7H_7O, 0.51), 109.0285 ($C_6H_5O_2$, 2.22), 110.0711 ($C_7H_8{}^2HO$, 0.26), 110.1075 ($C_8H_{12}{}^2H$, 0.62), 123.1137 ($C_9H_{11}{}^2H_2$, 1.12), 125.1294 ($C_9H_{13}{}^2H_2$, 0.63), 135.0438 ($C_8H_7O_2$, 0.20), 135.0802 ($C_9H_{11}O$, 0.50), 137.1292 ($C_{10}H_{13}{}^2H_2$, 1.37), 141.1241 ($C_9H_{13}{}^2H_2O$, 0.20), 148.1231 ($C_{11}H_{14}{}^2H$, 0.41), 161.1288 ($C_{12}H_{13}{}^2H_2$, 0.38), 163.1447 ($C_{12}H_{15}{}^2H_2$, 0.81), 173.0958 ($C_{12}H_{13}O$, 2.77), 179.1395 ($C_{12}H_{15}{}^2H_2O$, 0.11), 213.1270 ($C_{15}H_{17}O$, 0.25), 220.1770 ($C_{15}H_{18}{}^2H_3O$, 0.21), 242.1278 ($C_{16}H_{16}{}^2HO_2$, 1.53), 244.1436 ($C_{16}H_{18}{}^2HO_2$, 0.38), 256.1434 ($C_{17}H_{18}{}^2H_2O_2$, 12.22), 307.2008 ($C_{22}H_{23}{}^2H_2O$, 1.09), 380.2646 ($C_{26}H_{30}{}^2H_3O_2$, 7.70), 398.2751 ($C_{26}H_{32}{}^2H_3O_3$, 12.0).
16		$[M+H]^+$ 467.2429	109.0650 (C_7H_9O, 1.41), 109.1014 (C_8H_{13}, 2.09), 121.1013 (C_9H_{13}, 3.89), 123.0442 ($C_7H_7O_2$, 0.29), 125.0234 ($C_6H_5O_3$, 0.63), 135.0804 ($C_9H_{11}O$, 23.63), 137.0960 ($C_9H_{13}O$, 5.27), 147.1167 ($C_{11}H_{15}$, 2.20), 149.0960 ($C_{10}H_{13}O$, 15.81), 151.0387 ($C_8H_7O_3$, 0.32), 151.0750 ($C_9H_{11}O_2$, 0.26), 173.0960 ($C_{12}H_{13}O$, 3.24), 175.1116 ($C_{12}H_{15}O$, 4.50), 205.0863 ($C_{12}H_{13}O_3$, 0.34), 213.1272 ($C_{15}H_{17}O$, 6.51), 227.1064 ($C_{15}H_{15}O_2$, 2.78), 257.1169 ($C_{16}H_{17}O_3$, 3.82), 259.1325 ($C_{16}H_{19}O_3$, 0.39), 271.1325 ($C_{17}H_{19}O_3$, 2.43), 389.2106 ($C_{26}H_{29}O_3$, 35.74), 407.2212 ($C_{26}H_{31}O_4$, 100).
17		$[M+H]^+$ 457.2932	109.0649 (C_7H_9O, 0.34), 109.1013 (C_8H_{13}, 1.61), 111.0805 ($C_7H_{11}O$, 1.29), 113.0598 ($C_6H_9O_2$, 2.61), 121.1011 (C_9H_{13}, 0.79), 137.0959 ($C_9H_{13}O$, 1.03), 139.0751 ($C_8H_{11}O_2$, 1.09), 139.1115 ($C_9H_{15}O$, 0.63), 147.1165 ($C_{11}H_{15}$, 1.34), 151.1114 ($C_{10}H_{15}O$, 0.62), 175.1114 ($C_{12}H_{15}O$, 1.89), 177.1270 ($C_{12}H_{17}O$, 1.68), 215.1425 ($C_{15}H_{19}O$, 2.19), 217.1581 ($C_{15}H_{21}O$, 1.18), 245.1529 ($C_{16}H_{21}O_2$, 14.54), 247.1685 ($C_{16}H_{23}O_2$, 6.63), 259.1685 ($C_{17}H_{23}O_2$, 1.68), 353.2466 ($C_{24}H_{33}O_2$, 0.16), 379.2618 ($C_{26}H_{35}O_2$, 8.79), 397.2723 ($C_{26}H_{37}O_3$, 58.01), 457.2932 ($C_{28}H_{41}O_5$, 100).

epoxyazadiradione), **7** (1,2-dihydro-3β-hydroxyazadiradione), **8** (1,2-dihydro-3β-16β-dihydroxyazadiradione), **9** [(1,3-^{2}H)-1,2-dihydro-3β-hydroxyazadiradione], **10** [(1,3,16-^{2}H)-1,2-dihydro-3β-16β-dihydroxyazadiradione], **11** (3β-hydroxyazadiradione), **12** (3β-16β-dihydroxyazadiradione), **13** [(3-^{2}H)-3β-hydroxyazadiradione], **14** [(3,16-^{2}H)-3β-16β-dihydroxyazadir-

adione], **15** [(1,3,7-^{2}H)-1,2-dihydro-3β-hydroxy-7-deacetylazadiradione], and **17** (1,2,20,21,22,23-hexahydroazadiradione) and one isolated limonoid derivative **16**, (17β-hydroxyazadiradione), were individually subjected to MS/MS studies in 25% NCE. When the precursor ion of $[M + H]^+$ at m/z 451.2483 for azadiradione was subjected to MS/MS studies, the product ions

Table 2. Structure, Precursor Ion, and Their Product Ions (with Corresponding Chemical Formula and % Intensity) of Epoxyazadiradione (18) and Its Derivatives

No.	Structure	Precursor ion (m/z)	Product ions m/z (formula, % intensity at NCE 25%)
18		[M+H]$^+$ 467.2424	81.0340 (C_5H_5O, 14.89), 107.0859 (C_8H_{11}, 10.90), 109.0287 ($C_6H_5O_2$, 69.85), 121.1014 (C_9H_{13}, 13.0), 135.0805 ($C_9H_{11}O$, 40.30), 137.0961 ($C_9H_{13}O$, 20.14), 149.0961 ($C_{10}H_{13}O$, 100), 161.0961 ($C_{11}H_{13}O$, 16.22), 163.1117 ($C_{11}H_{15}O$, 14.70), 175.1117 ($C_{12}H_{15}O$, 15.22), 187.1117 ($C_{13}H_{15}O$, 9.58), 199.1117 ($C_{14}H_{15}O$, 11.75), 213.1272 ($C_{15}H_{17}O$, 16.54), 241.1584 ($C_{17}H_{21}O$, 9.52), 243.1377 ($C_{16}H_{19}O_2$, 9.30), 257.1169 ($C_{16}H_{17}O_3$, 16.59), 259.1326 ($C_{16}H_{19}O_3$, 10.74), 269.1896 ($C_{19}H_{25}O$, 14.45), 271.1325 ($C_{17}H_{19}O_3$, 26.06), 299.2001 ($C_{20}H_{27}O_2$, 15.02), 389.2106 ($C_{26}H_{29}O_3$, 17.68), 407.2211 ($C_{26}H_{31}O_4$, 73.04).
19		[M+H]$^+$ 425.2321	81.0340 (C_5H_5O, 45.23), 107.0858 (C_8H_{11}, 10.67), 109.0287 ($C_6H_5O_2$, 100), 121.1013 (C_9H_{13}, 17.86), 135.0805 ($C_9H_{11}O$, 28.08), 137.0961 ($C_9H_{13}O$, 28.93), 149.0961 ($C_{10}H_{13}O$, 37.71), 161.0960 ($C_{11}H_{13}O$, 15.33), 163.1116 ($C_{11}H_{15}O$, 13.11), 175.1116 ($C_{12}H_{15}O$, 22.36), 187.1116 ($C_{13}H_{15}O$, 19.65), 199.1116 ($C_{14}H_{15}O$, 10.83), 213.1272 ($C_{15}H_{17}O$, 12.37), 241.1584 ($C_{17}H_{21}O$, 3.93), 243.1376 ($C_{16}H_{19}O_2$, 4.44), 257.1169 ($C_{16}H_{17}O_3$, 17.14), 259.1326 ($C_{16}H_{19}O_3$, 2.77), 269.1895 ($C_{19}H_{25}O$, 33.16), 271.1325 ($C_{17}H_{19}O_3$, 12.45), 299.2000 ($C_{20}H_{27}O_2$, 11.12), 389.2105 ($C_{26}H_{29}O_3$, 22.52), 407.2210 ($C_{26}H_{31}O_4$, 83.81).
20		[M+H]$^+$ 423.2168	81.0341 (C_5H_5O, 41.26), 107.0859 (C_8H_{11}, 6.03), 109.0287 ($C_6H_5O_2$, 76.47), 121.1014 (C_9H_{13}, 6.51), 135.0805 ($C_9H_{11}O$, 31.35), 137.0961 ($C_9H_{13}O$, 11.59), 149.0961 ($C_{10}H_{13}O$, 25.40), 161.0961 ($C_{11}H_{13}O$, 7.84), 163.1117 ($C_{11}H_{15}O$, 3.74), 175.1117 ($C_{12}H_{15}O$, 32.21), 187.1117 ($C_{13}H_{15}O$, 7.43), 199.1117 ($C_{14}H_{15}O$, 6.45), 213.1272 ($C_{15}H_{17}O$, 14.55), 241.1587 ($C_{17}H_{21}O$, 1.76), 243.1379 ($C_{16}H_{19}O_2$, 1.97), 257.1169 ($C_{16}H_{17}O_3$, 1.84), 259.1335 ($C_{16}H_{19}O_3$, 0.29), 269.1897 ($C_{19}H_{25}O$, 17.0), 271.1326 ($C_{17}H_{19}O_3$, 1.15), 297.1845 ($C_{20}H_{25}O_2$, 38.24), 387.1949 ($C_{26}H_{27}O_3$, 11.22), 405.2055 ($C_{26}H_{29}O_4$, 67.58).
21		[M+H]$^+$ 469.2566	81.0339 (C_5H_5O, 11.18), 107.0856 (C_8H_{11}, 3.89), 109.0285 ($C_6H_5O_2$, 44.81), 121.1011 (C_9H_{13}, 5.09), 135.0802 ($C_9H_{11}O$, 2.37), 137.0958 ($C_9H_{13}O$, 6.29), 139.1114 ($C_9H_{15}O$, 3.12), 151.1114 ($C_{10}H_{15}O$, 8.80), 161.0957 ($C_{11}H_{13}O$, 5.0), 163.1113 ($C_{11}H_{15}O$, 5.0), 175.1113 ($C_{12}H_{15}O$, 3.26), 177.1270 ($C_{12}H_{17}O$, 3.78), 187.1113 ($C_{13}H_{15}O$, 2.06), 199.1115 ($C_{14}H_{15}O$, 2.27), 213.1267 ($C_{15}H_{17}O$, 5.82), 241.1579 ($C_{17}H_{21}O$, 1.45), 243.1374 ($C_{16}H_{19}O_2$, 2.73), 257.1164 ($C_{16}H_{17}O_3$, 43.91), 259.1320 ($C_{16}H_{19}O_3$, 22.61), 271.2047 ($C_{19}H_{27}O$, 4.93), 271.1319 ($C_{17}H_{19}O_3$, 11.64), 301.2150 ($C_{20}H_{29}O_2$, 13.06), 391.2252 ($C_{26}H_{31}O_3$, 29.40), 409.2358 ($C_{26}H_{33}O_4$, 100).

at m/z 107.0496, 109.0288, 109.0652, 109.1016, 121.1015, 135.0443, 135.0806, 137.0963, 147.1170, 149.0963, 173.0962, 175.1119, 213.1274, 241.1223, 243.1379, 255.1379, 349.2159, 373.2161, and 391.2267 were obtained (Table 1). Many of the product ions obtained for **2** were present for its functionally modified analogs **1** and **3−17**. However, due to various modifications such as deacetylation, carbonylation, and reduction in carbonyl/oleofinic double bond/furan ring, the m/z values of the product ions in the analogs varied with respect to product ions obtained for **2**. In brief, the deacetylation and carbonylation at C7 of **2** produced analogs **3** and **4**, respectively. The $\Delta^{1,2}$ reduction of **2** formed analog **5**. The epoxidation at the A-ring in **2** generated the analog **6**. The reduction at the C3 carbonyl and the $\Delta^{1,2}$ double bond of **2** formed analog **7**. Further, reduction at the C16 of **7** generated analog **8**. The derivatives **9** and **10** are isotopologs of **7** and **8**, respectively. The reduction at the C3 carbonyl of **2** formed analog **11**. The reduction at the C16 carbonyl of **11** formed analog **12**. The derivatives **13** and **14** are isotopologs of **11** and **12**, respectively. The reduction at the C3 carbonyl and the $\Delta^{1,2}$ double bond of **3** formed analog **15** which was deuterated at C1, C3, and C7. The C17 hydroxylation of **2** generated analog **16**. The reduction of the furan ring in **5** formed analog **17** (Scheme 1).

The structure and mechanism of formation of the product ions originating from the precursor ion of **2** and the corresponding product ions generated in the analogs are discussed in detail. The product ion of highest intensity at m/z 391.2267 (100%) of **2** was formed by the loss of the acetoxy group at the B-ring by inductive cleavage as reported in the HighChem Fragmentation Library, which was favored in analogs **5−14**, **16**, and **17** (Figures 6 and S174). The dehydration and carbonyl reduction at the B-ring in analogs **3**, **15**, and **4**, respectively, yielded the corresponding product ions. The corresponding product ions appeared at m/z 391.2264 in **3**; at m/z 407.2213 in **4**, **6**, and **16**; at m/z 393.2416 in **5** and **11**; at m/z 395.2565 in **7** and **12**; and at m/z 397.2727 in **8** and **17**. Further, this proposed fragmentation pathway was verified by the presence of the product ion with increased mass in isotopologs at m/z 397.2727 in **9** and **14**; at m/z 400.2917 in **10**; at m/z 394.2482 in **13**; and at m/z 398.2751 in **15**.

The protonation initiated at C16 carbonyl followed by the neutral loss of water molecule and acetic acid, generated the product ion at m/z 373.2161 (19.17%) of **2**, and this route was favored by analogs **5−14** and **17** (Figures 6 and S174), whereas in analogs **3** and **15**, the C16 carbonyl protonation was followed by dehydration at the B- and D-rings. Also, in analog **4**, the C16 carbonyl protonation and dehydration formed the corresponding product ion. The C7 deacetoxylation and C17 dehydration in analog **16** formed the corresponding product ion. The product ion at m/z 373.2161 of **2** appeared at m/z 373.2158 in **3**; at m/z 389.2106 in **4**, **6**, and **16**; at m/z 375.2311 in **5** and **11**; at m/z 377.2460 in **7** and **12**; and at m/z 379.2624 in **8** and **17**. This fragmentation pathway was confirmed by the presence of product ion with increased mass in isotopologs at m/z 379.2624 in **9** and **14**; at m/z 382.2809 in **10**; at m/z 376.2376 in **13**; and at m/z 380.2646 in **15**.

The product ion at m/z 349.2159 (11.84%) of **2** was formed through protonation mediated cleavage of the A-ring followed

Table 3. Structure, Precursor Ion, and Their Product Ions (with Corresponding Chemical Formula and % Intensity) of Gedunin (22) and Its Derivatives

No.	Structure	Precursor ion (m/z)	Product ions m/z (formula, % intensity at NCE 25 %)
22		[M+H]⁺ 483.2379	95.0132 ($C_5H_3O_2$, 36.80), 119.0858 (C_9H_{11}, 13.05), 135.0806 ($C_9H_{11}O$, 44.07), 137.0962 ($C_9H_{13}O$, 100), 149.0962 ($C_{10}H_{13}O$, 16.84), 161.0597 ($C_{10}H_9O_2$, 49.07), 175.0754 ($C_{11}H_{11}O_2$, 13.56), 175.1117 ($C_{12}H_{15}O$, 5.09), 253.1585 ($C_{18}H_{21}O$, 10.93), 267.1377 ($C_{18}H_{19}O_2$, 31.34), 293.1169 ($C_{19}H_{17}O_3$, 16.56), 379.2263 ($C_{25}H_{31}O_3$, 15.04), 423.2161 ($C_{26}H_{31}O_5$, 34.74).
23		[M+H]⁺ 441.2265	95.0131 ($C_5H_3O_2$, 27.05), 119.0855 (C_9H_{11}, 7.51), 135.0803 ($C_9H_{11}O$, 26.54), 137.0959 ($C_9H_{13}O$, 52.10), 149.0959 ($C_{10}H_{13}O$, 27.20), 161.0595 ($C_{10}H_9O_2$, 25.67), 175.0751 ($C_{11}H_{11}O_2$, 10.73), 175.1115 ($C_{12}H_{15}O$, 8.12), 253.1582 ($C_{18}H_{21}O$, 21.76), 267.1374 ($C_{18}H_{19}O_2$, 11.21), 293.1167 ($C_{19}H_{17}O_3$, 7.33), 379.2261 ($C_{25}H_{31}O_3$, 13.09), 423.2158 ($C_{26}H_{31}O_5$, 73.62).
24		[M+H]⁺ 439.2107	95.0130 ($C_5H_3O_2$, 18.47), 119.0854 (C_9H_{11}, 2.23), 135.0802 ($C_9H_{11}O$, 22.32), 137.0958 ($C_9H_{13}O$, 37.72), 149.0958 ($C_{10}H_{13}O$, 7.94), 161.0594 ($C_{10}H_9O_2$, 41.40), 175.0750 ($C_{11}H_{11}O_2$, 7.15), 175.1114 ($C_{12}H_{15}O$, 8.66), 253.1580 ($C_{18}H_{21}O$, 1.23), 267.1377 ($C_{18}H_{19}O_2$, 0.75), 293.1168 ($C_{19}H_{17}O_3$, 0.23), 395.2208 ($C_{25}H_{31}O_4$, 9.13), 421.1999 ($C_{26}H_{29}O_5$, 8.07).
25		[M+H]⁺ 485.2526	95.0130 ($C_5H_3O_2$, 32.50), 121.1011 (C_9H_{13}, 8.96), 135.0802 ($C_9H_{11}O$, 5.01), 137.0958 ($C_9H_{13}O$, 3.27), 139.1115 ($C_9H_{15}O$, 4.86), 151.1114 ($C_{10}H_{15}O$, 2.32), 161.0594 ($C_{10}H_9O_2$, 92.13), 175.0751 ($C_{11}H_{11}O_2$, 60.53), 177.1270 ($C_{12}H_{17}O$, 2.58), 255.1737 ($C_{18}H_{23}O$, 14.49), 267.1375 ($C_{18}H_{19}O_2$, 1.94), 293.1171 ($C_{19}H_{17}O_3$, 0.43), 381.2415 ($C_{25}H_{33}O_3$, 20.17), 425.2313 ($C_{26}H_{33}O_5$, 100).
26		[M+H]⁺ 499.2433	95.0132 ($C_5H_3O_2$, 23.24), 119.0856 (C_9H_{11}, 7.92), 135.0804 ($C_9H_{11}O$, 3.89), 137.0961 ($C_9H_{13}O$, 2.45), 149.0961 ($C_{10}H_{13}O$, 3.31), 161.0595 ($C_{10}H_9O_2$, 13.26), 175.0753 ($C_{11}H_{11}O_2$, 6.20), 175.1111 ($C_{12}H_{15}O$, 2.02), 267.1389 ($C_{18}H_{19}O_2$, 0.43), 269.1533 ($C_{18}H_{21}O_2$, 11.58), 293.1163 ($C_{19}H_{17}O_3$, 1.35), 395.2214 ($C_{25}H_{31}O_4$, 1.46), 439.2110 ($C_{26}H_{31}O_6$, 32.52).
27		[M+H]⁺ 457.2218	95.0132 ($C_5H_3O_2$, 31.58), 119.0857 (C_9H_{11}, 9.35), 135.0805 ($C_9H_{11}O$, 5.67), 137.0960 ($C_9H_{13}O$, 2.95), 149.0959 ($C_{10}H_{13}O$, 5.09), 161.0596 ($C_{10}H_9O_2$, 16.68), 175.0755 ($C_{11}H_{11}O_2$, 6.20), 175.1112 ($C_{12}H_{15}O$, 2.42), 267.1372 ($C_{18}H_{19}O_2$, 0.79), 269.1536 ($C_{18}H_{21}O_2$, 12.39), 293.1169 ($C_{19}H_{17}O_3$, 0.82), 395.2215 ($C_{25}H_{31}O_4$, 0.84), 439.2110 ($C_{26}H_{31}O_6$, 30.34).
28		[M+H]⁺ 487.2670	95.0129 ($C_5H_3O_2$, 15.74), 121.1011 (C_9H_{13}, 20.18), 123.1167 (C_9H_{15}, 9.56), 135.0801 ($C_9H_{11}O$, 0.80), 135.1165 ($C_{10}H_{15}O$, 18.82), 139.1115 ($C_9H_{15}O$, 1.52), 161.0593 ($C_{10}H_9O_2$, 23.14), 161.1325 ($C_{12}H_{17}$, 3.15), 175.0749 ($C_{11}H_{11}O_2$, 13.20), 257.1890 ($C_{18}H_{25}O$, 3.35), 269.1527 ($C_{18}H_{21}O_2$, 1.99), 297.1472 ($C_{19}H_{21}O_3$, 0.77), 383.2568 ($C_{25}H_{35}O_3$, 2.70), 427.2461 ($C_{26}H_{35}O_5$, 32.42).
29		[M+H]⁺ 489.2797	95.0130 ($C_5H_3O_2$, 18.79), 122.1075 ($C_9H_{12}{}^2H$, 11.33), 125.1294 ($C_9H_{13}{}^2H_2$, 5.49), 135.0804 ($C_9H_{11}O$, 0.78), 137.1292 ($C_{10}H_{13}{}^2H_2$, 8.27), 141.1238 ($C_9H_{13}{}^2H_2O$, 0.49), 161.0594 ($C_{10}H_9O_2$, 28.42), 163.1446 ($C_{12}H_{15}{}^2H_2$, 3.05), 175.0750 ($C_{11}H_{11}O_2$, 12.96), 259.2017 ($C_{18}H_{23}{}^2H_2O$, 3.00), 270.1586 ($C_{18}H_{20}{}^2HO_2$, 1.62), 299.1597 ($C_{19}H_{19}{}^2H_2O_3$, 0.12), 385.2692 ($C_{25}H_{33}{}^2H_2O_3$, 3.10), 429.2588 ($C_{26}H_{33}{}^2H_2O_5$, 39.10).
30		[M+H]⁺ 499.2329	95.0133 ($C_5H_3O_2$, 31.57), 133.0650 (C_9H_9O, 22.54), 135.0806 ($C_9H_{11}O$, 48.33), 137.0962 ($C_9H_{13}O$, 19.56), 149.0962 ($C_{10}H_{13}O$, 20.46), 161.0598 ($C_{10}H_9O_2$, 100), 175.0756 ($C_{11}H_{11}O_2$, 24.99), 175.1116 ($C_{12}H_{15}O$, 12.16), 253.1584 ($C_{18}H_{21}O$, 4.22), 265.1241 ($C_{18}H_{17}O_2$, 2.77), 293.1167 ($C_{19}H_{17}O_3$, 2.0), 377.2114 ($C_{25}H_{29}O_3$, 12.73), 421.2007 ($C_{26}H_{29}O_5$, 14.69).
31		[M+H]⁺ 499.2326	95.0133 ($C_5H_3O_2$, 100), 133.0649 (C_9H_9O, 10.51), 135.0806 ($C_9H_{11}O$, 89.94), 137.0961 ($C_9H_{13}O$, 51.24), 149.0961 ($C_{10}H_{13}O$, 64.88), 161.0598 ($C_{10}H_9O_2$, 20.32), 175.0754 ($C_{11}H_{11}O_2$, 18.94), 175.1118 ($C_{12}H_{15}O$, 22.61), 253.1585 ($C_{18}H_{21}O$, 12.56), 265.1222 ($C_{18}H_{17}O_2$, 4.75), 293.1171 ($C_{19}H_{17}O_3$, 1.62), 377.2107 ($C_{25}H_{29}O_3$, 40.29), 421.2005 ($C_{26}H_{29}O_5$, 24.22).

by removal of the C16 carbonyl oxygen as reported in the HighChem Fragmentation Library. This fragmentation pathway was supported by the presence of product ions at the same mass in analogs **5**−**7** and **11**−**13**; at m/z 305.1895 in **3**; at m/z 321.1845 in **4**; and at m/z 353.2466 in **17**. The mass differences observed in the analogs were associated with B-ring dehydration, an intact C7 carbonyl, and a reduced furan ring, respectively (Figures 4 and S174). Further, this fragmentation pathway was validated by the presence of product ions with increased mass in isotopologs at m/z 350.2224 in **9** and **14** and at m/z 307.2008 in

15. However, no corresponding product ions were detected in analogs **8** and **10** due to reduced C16 carbonyl and conjugated carbonyl moiety at the A-ring as well as in analog **16** due to the C17 hydroxyl moiety.

The B-ring cleavage in the product ion at m/z 391.2267 of **2** generated another product ion at m/z 255.1379 (33.24%) (Figures 6 and S174). This fragmentation pathway was favored by the presence of product ions at the same mass in analogs **3**, **5**−**7**, **9**, **11**, and **13**; at m/z 253.1220 in **4**; at m/z 239.1426 in **8** and **12**; at m/z 271.1325 in **16**; and at m/z 259.1685 in **17**. The
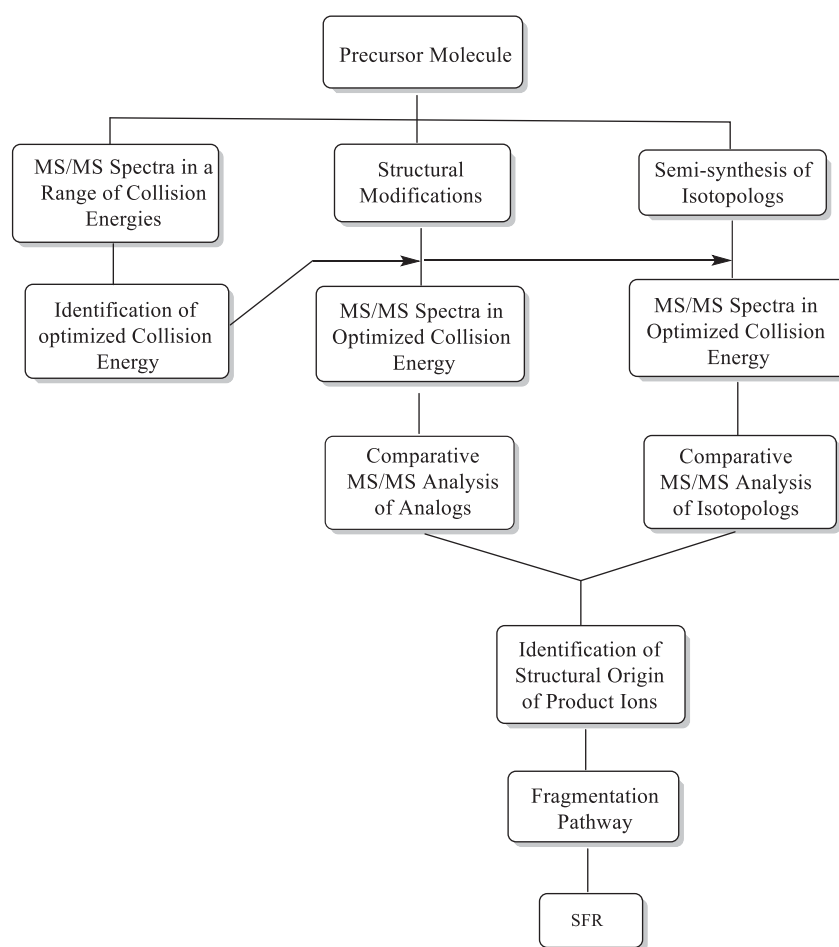
Figure 3. Flowchart depicting the elucidation of structure−fragment relationships (SFRs) in complex natural organic molecules.

mass differences observed in the analogs were associated with dehydration at the B/D-rings, an additional C17 hydroxyl moiety and a reduced furan ring. This fragmentation pathway was evident by the presence of the product ion with increased mass in the isotopologs at m/z 240.1488 in **10** and **14** and at m/z 256.1434 in **15**.

The product ions at m/z 243.1379 (21.78%) and 241.1223 (21.46%) of **2** were formed by protonation initiated at the D-ring and subsequent cleavages of A-, B-, and C-rings (Figure 5). These fragmentation pathways of product ions at m/z 243.1379 and 241.1223 of **2** were supported by the presence of product ions at the same mass in analogs **3**−**7**, **9**, **11**, and **13**; at m/z 227.1426 and 225.1270 in **8** and **12**; at m/z 259.1325, and 257.1169 in **16**; and at m/z 247.1685 and 245.1529 in **17**. The mass differences observed in the analogs were associated with dehydration at the B/D-rings, an additional C17 hydroxyl moiety, and a reduced furan ring. This proposed fragmentation route was evident by the presence of product ion with increased mass in isotopologs at m/z 228.1489 and 226.1332 in **10** and **14** and at m/z 244.1436 and 242.1278 in **15** corresponding to product ions at m/z 243.1379 and 241.1223 of **2**, respectively.

For the product ion at m/z 213.1274 (15.98%) of **2**, two structurally different product ions were formed with the same elemental compositions (**213a**, **213b**) (Figures 4 and 6). Protonation initiated at the D-ring followed by subsequent cleavages led to the formation of product ion at m/z 213.1274 (**213a**), and this was supported by the formation of products ions at the same mass in analogs **3**, **4**, **6**, and **16**; at m/z 215.1428

in **5**, **11**, **12**, and **17**; and at m/z 217.1581 in **7** and **8**. The mass differences observed in the analogs were associated with the reduction in the $\Delta^{1,2}$ double bond/C3 carbonyl and C3 hydroxyl moiety. This fragmentation route was evidenced by the presence of product ion with increased mass in isotopologs at m/z 219.1714 in **9** and **10** and at m/z 216.1469 in **13** and **14**. The product ion at m/z 213.1274 (**213b**) originated through two different routes. In one mechanism it was formed by protonation initiated at the A-ring following cleavages of the A- and B-rings. In another route its formation was initiated by deacetoxylation at C7 followed by the retro-Diels−Alder mechanism. This fragmentation route was favored by the presence of product ions at the same mass in analogs **3**−**9**, **11**−**13**, and **15**; at m/z 227.1064 in **16**; and at m/z 217.1581 in **17**. The mass differences observed in the analogs were associated with an additional C17 hydroxyl moiety and a reduced furan ring, respectively. Further, the increased mass in the product ion of isotopologs at m/z 214.1333 in **10** and **14** confirmed the fragmentation mechanism.

For the product ion at m/z 175.1119 (10.17%) of **2**, two structurally different product ions were formed with the same elemental compositions (**175a**, **175b**) (Figures 5 and 6). The product ion **175a** of **2** was formed through protonation initiated at the D-ring followed by a 1,3 shift and subsequent cleavages. This fragmentation route was favored by the appearance of product ion at the same mass in analogs **3**−**6**, **16**, and **17** and at m/z 177.1268 in analogs **7**, **8**, **11**, and **12**, and the proposed fragmentation route was confirmed by the presence of product ion at m/z 178.1355 in their respective isotopologs **9**, **10**, **13**, **14**
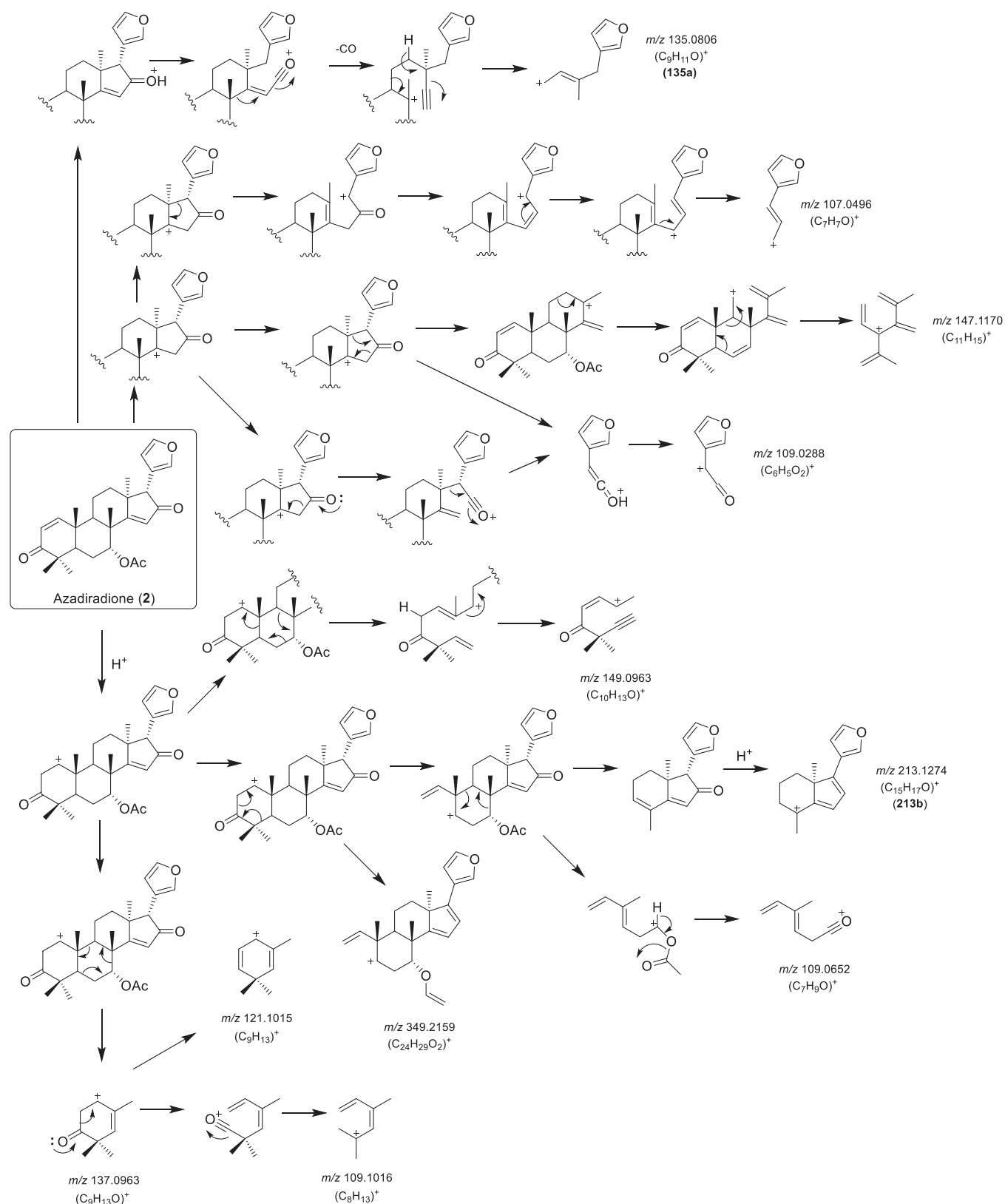
Figure 4. Tentative fragmentation pattern obtained from the product ion scan of the precursor ion of azadiradione at m/z 451.2483.

as well as at m/z 179.1395 in the C3, C7 deuterated analog **15**. The mass differences observed in the analogs were due to the C3 carbonyl reduction. The product ions at m/z 175.1119 (10.17%) (**175b**) and 173.0962 (14.90%) (**173a**) of **2** were generated by protonation initiated at the D-ring and subsequent

cleavage of the B-, C-, and D-rings (Figure 5). This fragmentation route for the product ions at m/z 175.1119 (**175b**) and 173.0962 (**173a**) of **2** was supported by the presence of product ions at the same mass in analogs **3**, **4**, **6**, and **16**; at m/z 177.1270 and 175.1114 in **5**, **11**, **12**, and **17**; and at
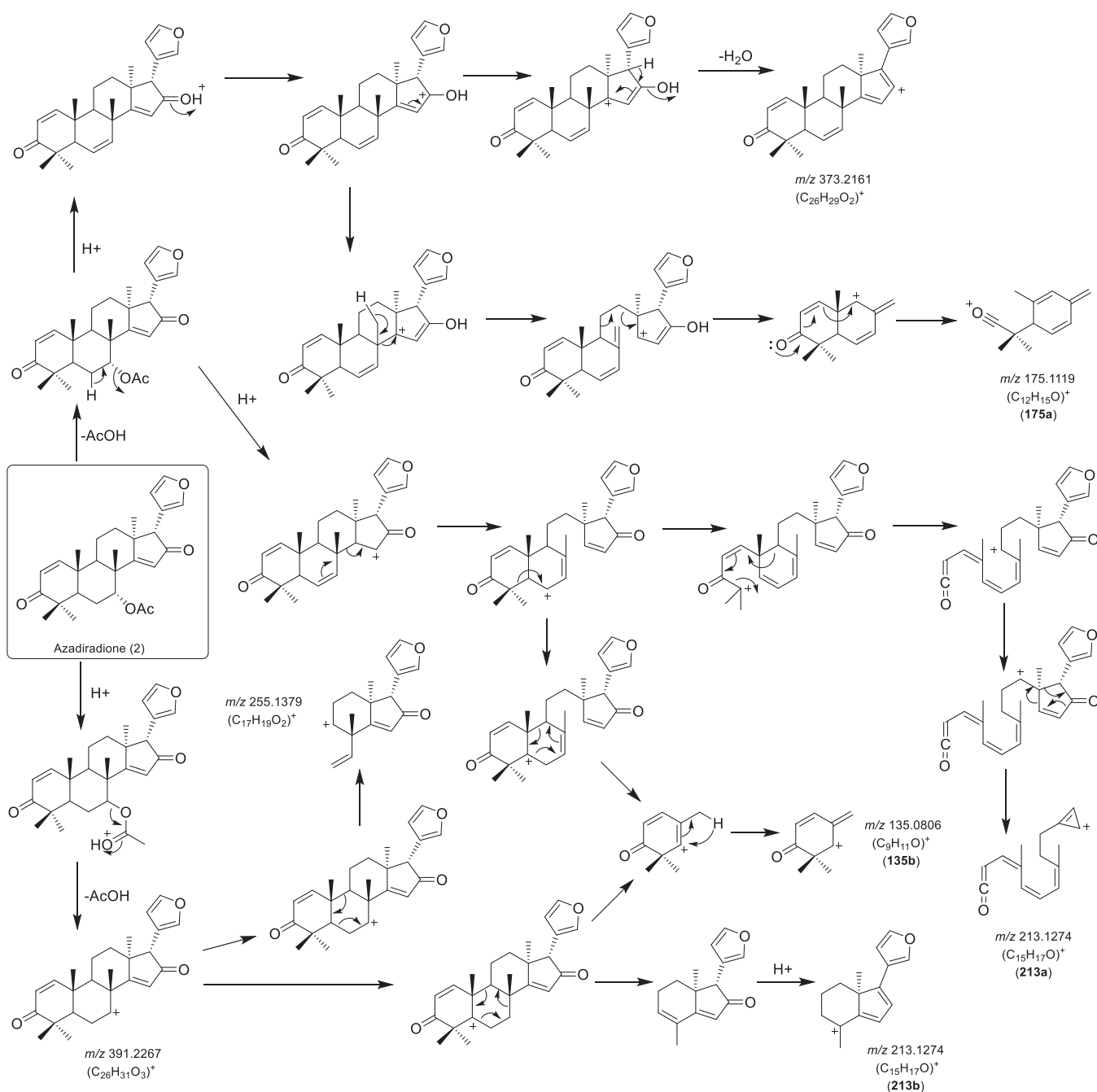
Figure 5. Tentative fragmentation pattern obtained from the product ion scan of the precursor ion of azadiradione at *m/z* 451.2483.

m/z 161.1321 and 159.1165 in **7** and **8**, respectively. The mass differences observed in the analogs were associated with a reduction in the $\Delta^{1,2}$ double bond/C3 carbonyl. This fragmentation route was validated by the presence of product ions with increased mass in the isotopologs, i.e., at *m/z* 178.1333 and 176.1178 in **13** and **14** and at *m/z* 163.1451 and 161.1322 in **9**, **10**, and **15** corresponding to product ions at *m/z* 175.1119 (**175b**) and 173.0962 (**173a**) of **2**, respectively. The D-ring protonation followed by subsequent cleavage led to the formation of the product ion at *m/z* 173.0962 (**173b**) of **2**. This fragmentation route was supported by the presence of product ions at the same mass in analogs **3–9**, **11–13**, and **15**; at *m/z* 205.0863 in **16**; and at *m/z* 177.1270 in **17**. The mass differences observed in these analogs were associated with the additional C17 hydroxyl moiety and a reduced furan ring, respectively. Further, it was evident by the presence of product ion with increased mass at *m/z* 174.1022 in isotopologs **10** and **14** which are C16 deuterated.

After the A-ring protonation, subsequent cleavages formed the product ion at *m/z* 149.0963 (23.37%) of **2** whereas retro-Diels–Alder rearrangement after the A-ring protonation led to the formation of product ion at *m/z* 137.0963 (25.80%) of **2** (Figure 4). Both mechanisms were supported by the presence of product ions at the same mass in analogs **3**, **4**, **6**, and **16** and varied in others due to structural modifications. The fragmentation pathway for the product ions at *m/z* 149.0963 and 137.0963 of **2** appeared at *m/z* 151.1114 and 139.1117 in **5**, **11**, **12**, and **17** and at *m/z* 135.1166 and 123.1167 in **7** and **8**, respectively. The mass differences observed in the analogs were due to the reduction in the $\Delta^{1,2}$ double bond/C3 carbonyl. These fragmentation routes were further evidenced by the presence of product ions with increased mass in isotopologs at *m/z* 152.1177 and 140.1180 in **13** and **14** and *m/z* 137.1296 and 125.1297 in **9**, **10**, and **15** corresponding to product ions at *m/z* 149.0963 and 137.0963 of **2**, respectively.

Figure 6. Tentative fragmentation pattern obtained from the product ion scan of the precursor ion of azadiradione at m/z 451.2483

The product ion generated at m/z 147.1170 (10.61%) in **2** was formed through the D-ring protonation following cleavages and was supported by the presence of product ions at the same mass in analogs **3–14**, **16**, and **17** as well as in C7 deuterated analog **15** where it appeared at m/z 148.1231 (Figure 4).

For the product ion at m/z 135.0806 (19.72%) two structurally different fragments (**135a**, **135b**) with the same elemental compositions were generated (Figures 4 and 6). The mechanism of formation of the product ion at m/z 135.0806 (**135a**) of **2** was initiated through the D-ring protonation following successive cleavages as reported earlier on the ring-opening fragmentation mechanism for the lactone moiety.[39,40] This fragmentation pathway was supported by the presence of product ions at the same mass in analogs **3–15**; at m/z 151.0750 in **16**; and at m/z 139.1115 in **17**. The mass differences observed

in the analogs were due to an additional C17 hydroxyl moiety and a reduced furan ring, respectively, whereas the product ion at m/z 135.0806 (**135b**) of **2** was formed through deacetoxylation at C7 or protonation initiated at the D-ring and both the routes then involve a retro-Diels–Alder mechanism followed by a 1,3 shift. This fragmentation route was favored by the presence of product ions at the same mass in analogs **3**, **4**, **6**, and **16**; at m/z 137.0960 in **5** and **17**; at m/z 139.1115 in **7** and **8**; and at m/z 137.1296 in **11** and **12**. The mass differences observed in the analogs were associated with the reduction in the $\Delta^{1,2}$ double bond/C3 carbonyl and with C3 hydroxylation. Further, the fragmentation pathway was evident from the increased mass in product ion of isotopologs at m/z 141.1245 in **9**, **10**, and **15** and at m/z 138.1024 in **13** and **14**.
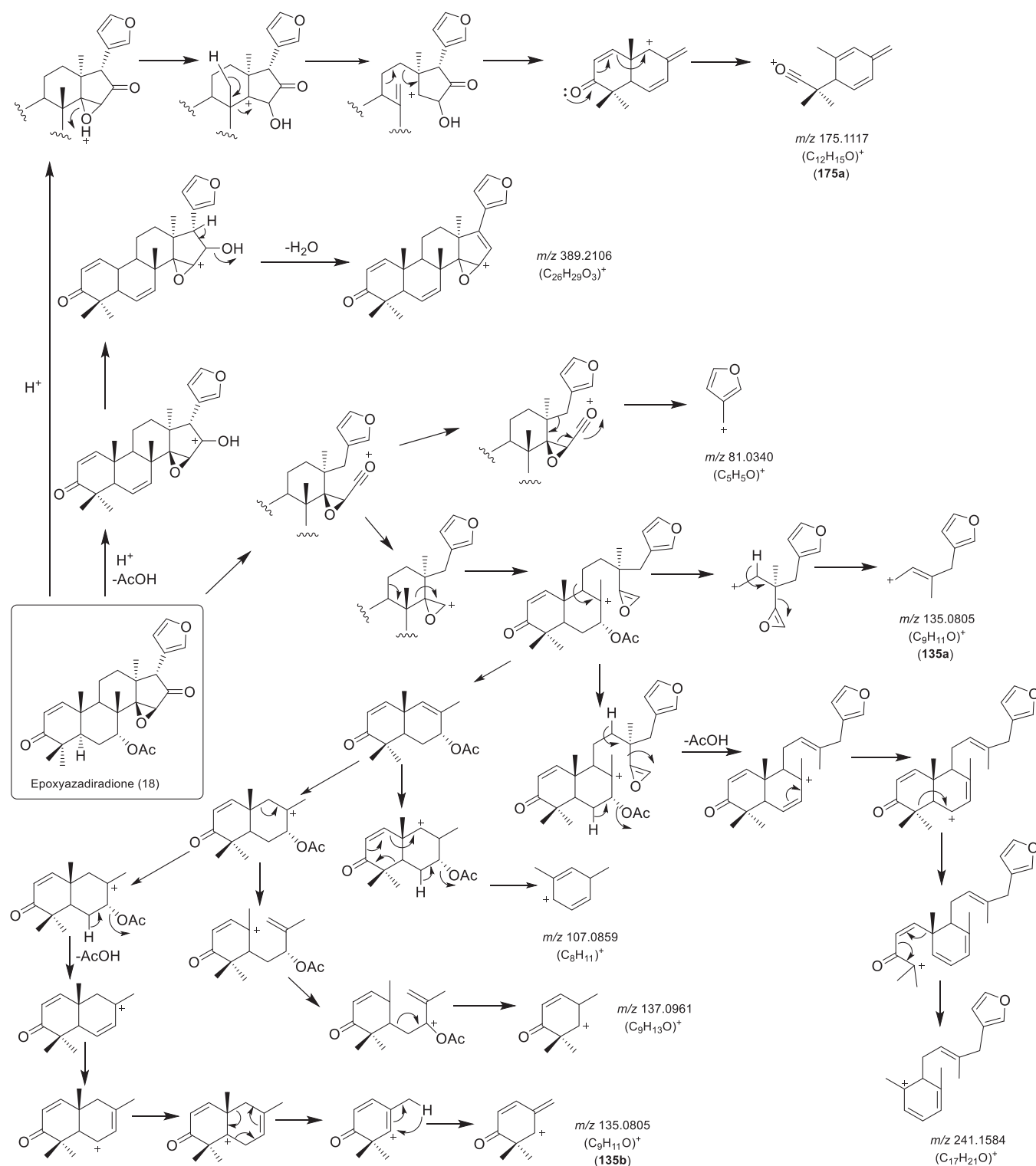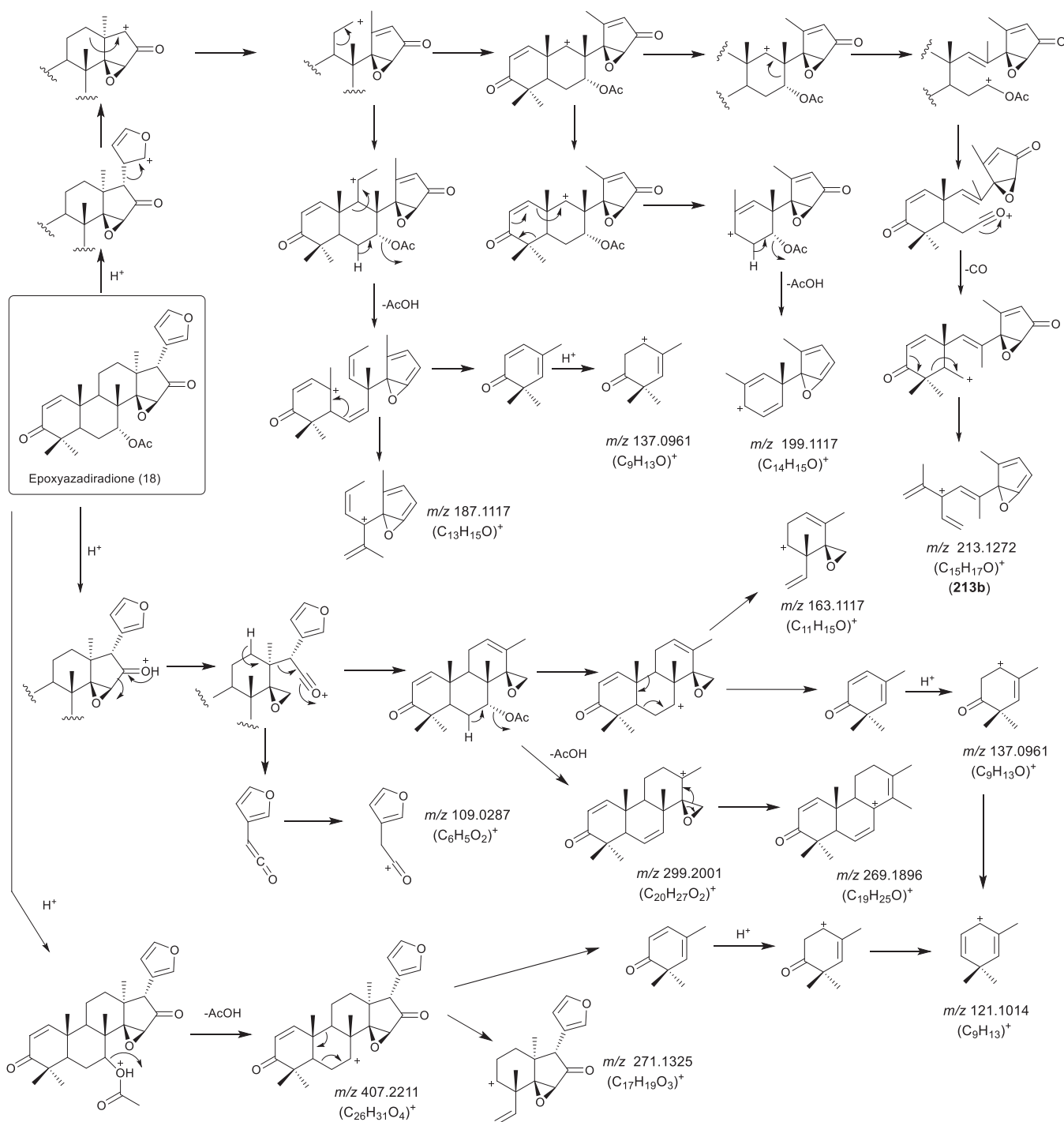
Figure 7. Tentative fragmentation pattern obtained from the product ion scan of the precursor ion of epoxyazadiradione at m/z 467.2424.

The D-ring protonation following cleavages formed the product ion at m/z 135.0443 (16.02%) from the precursor ion of **2** (Figure 5). This fragmentation pathway was supported by the presence of product ions at the same mass in analogs **3−7, 9, 11, 13,** and **15**; at m/z 119.0492 in **8** and **12**; at m/z 151.0387 in **16**; and at m/z 139.0751 in **17**. The mass differences observed in the analogs were due to dehydration, additional C17 hydroxyl moiety and reduced furan ring. This fragmentation pathway was

confirmed by the increased mass in product ions at m/z 120.0554 in isotopologs **10** and **14**.

The product ion at m/z 121.1015 (14.98%) of **2** was formed from the product ion at m/z 137.0963 and was supported by the presence of product ions at the same mass in analogs **3−8, 11, 12, 16,** and **17** (Figure 4). This fragmentation route was evident by the increased mass of product ions in isotopologs at m/z 123.1137 in **9, 10,** and **15** and at m/z 122.1077 in **13, 14**.
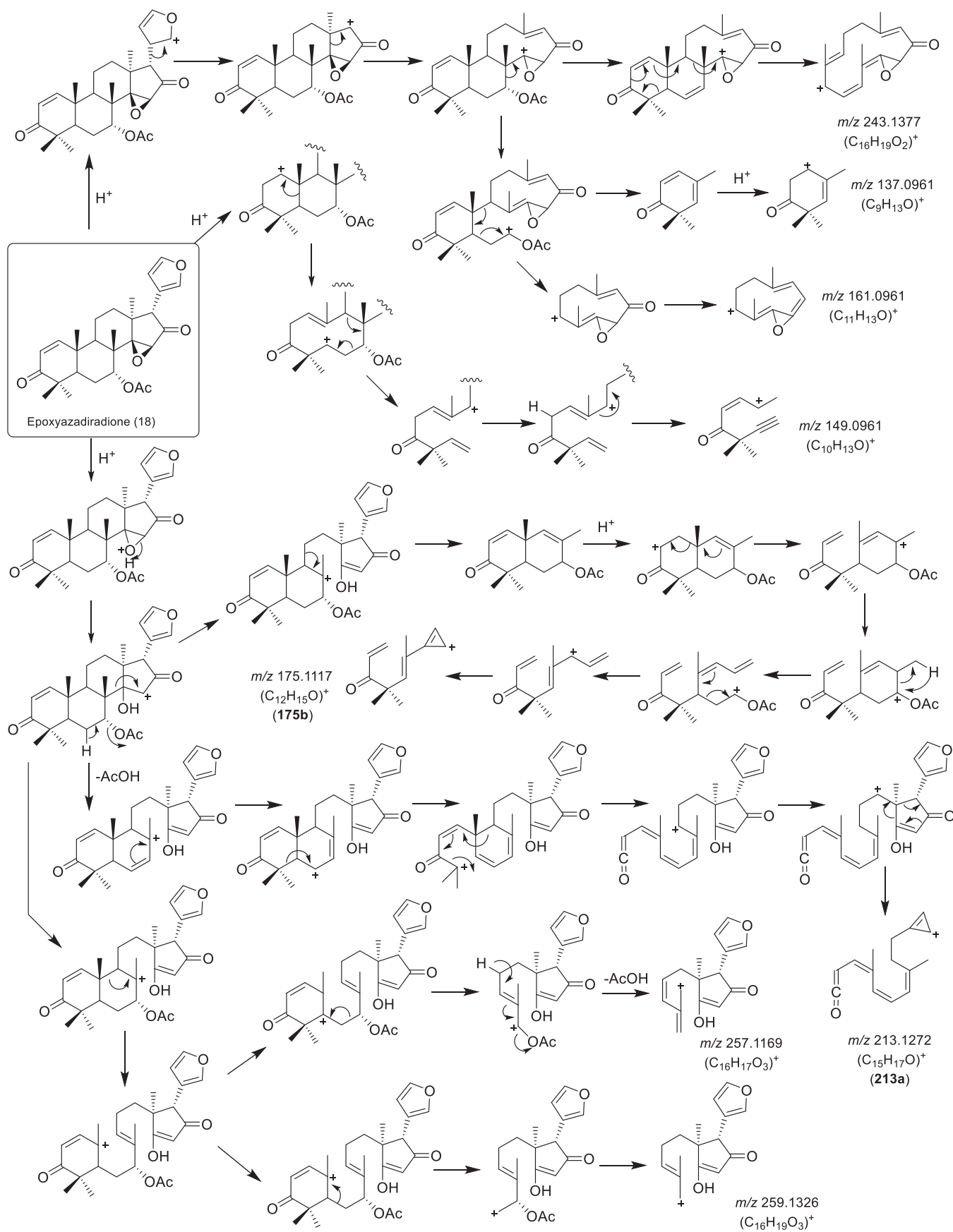
Figure 8. Tentative fragmentation pattern obtained from the product ion scan of the precursor ion of epoxyazadiradione at m/z 467.2424.

The cleavage of product ion at m/z 137.0963 of **2** generated another product ion at m/z 109.1016 (11.13%) and the product ion at m/z 109.0652 (11.05%) of **2** was generated through the A-ring protonation with fragment ion containing cleaved portions of A- and B-rings (Figure 4). Both these fragmentation pathways were supported by the presence of the same-mass product ions in analogs **3−8, 11−14, 16**, and **17**, which was confirmed by the increased mass of product ion in deuterated analogs **9, 10**, and **15**.

The lower mass product ions at m/z 109.0288 (16.40%) and 107.0496 (22.98%) of **2** were generated through the D-ring protonation with a fragment ion containing furan ring (Figure

4). The fragmentation pathway of product ion at m/z 109.0288 of **2** was supported by the presence of the same-mass product ions in analogs **3−7, 9, 11, 13**, and **15**; at m/z 95.0495 in **8** and **12**; at m/z 125.0234 in **16**; and at m/z 113.0598 in **17**. The mass differences observed in the analogs were associated with C16 dehydroxylation, additional C17 hydroxyl moiety and reduced furan ring. This fragmentation pathway was evident with the increased mass of product ions in isotopologs at m/z 96.0557 in **10** and **14**. The fragmentation pathway of product ion at m/z 107.0496 of **2** was supported by the presence of the same-mass product ions in analogs **3−9, 11−13**, and **15**; at m/z 123.0442 in **16**; and at m/z 111.0805 in **17**. The mass differences observed in

Figure 9. Tentative fragmentation pattern obtained from the product ion scan of the precursor ion of epoxyazadiradione at m/z 467.2424.

the analogs were associated with the additional C17 hydroxyl moiety and reduced furan ring, respectively. This fragmentation pathway was confirmed by the presence of increased mass in product ions of isotoplogs at m/z 108.0556 in **10** and **14**.

To further validate our proposed fragmentation pathway we subjected azadirone (**1**) to MS/MS fragmentation under the same parameters and established a tentative fragmentation pattern. Azadirone (**1**) is a natural analog of **2** isolated from the Neem fruit, which differed only at C16 position in the D-ring. From the precursor ion at m/z 437.2687 of **1**, the product ions at m/z 95.0495, 107.0495, 109.0651, 109.1014, 121.1013, 121.0650, 135.0805, 137.0961, 147.1168, 149.0960, 175.1116, 213.1272, 215.1428, 227.1427, 229.1584, 241.1584, and 377.2468 were generated. The initiation or termination of fragmentation involving the D-ring plays a key role in generating the product ions of **1** and **2**. The product ions at m/z 213.1274 (**213a**), 149.0963, 147.1170, 137.0963, 135.0806 (**135b**), 121.1015, 109.1016, 109.0652, and 107.0496 of **2** appeared at the same mass in **1**. The product ion at m/z 109.0288 ($C_6H_5O_2$) of **2** appeared at m/z 95.0495 (43.86%) in **1**, because the oxygen atom at C16 was absent in **1**, thus supporting the proposed fragmentation pathway. The structure and the mechanism of formation of the product ions at m/z 377.2468, 241.1584, 229.1584, 227.1427, 215.1428, 175.1116, and 121.1013 originating from the precursor ion of **1**, due to involvement of the D-ring, occurs by a similar mechanism of the product ions at m/z 391.2267, 255.1379, 243.1379, 241.1223, 213.1274 (**213b**), 173.0962 (**173b**), and 135.0443, respectively generated from the precursor ion **2**. The product ions at m/z 373.2161, 349.2159, 175.1119 (**175a**, **175b**), 173.0962 (**173a**), and 135.0806 (**135a**) of **2** were not detected in **1** due to the involvement of the C16 carbonyl at the D-ring in the fragmentation mechanism.

2.5.2. MS/MS Characterization of Epoxyazadiradione (18) and Its Derivatives. The tentative fragmentation pattern obtained by the HCD-MS/MS of the precursor ion of epoxyazadiradione (**18**) having the precursor ion of $[M + H]^+$ at m/z 467.2424 was subjected to MS/MS studies in 25% NCE, which generated product ions at m/z 81.0340, 107.0859, 109.0287, 121.1014, 135.0805, 137.0961, 149.0961, 161.0961, 163.1117, 175.1117, 187.1117, 199.1117, 213.1272, 241.1584, 243.1377, 257.1169, 259.1326, 269.1896, 271.1325, 299.2001, 389.2106, and 407.2211 (Table 2), is represented in Figures 7, 8, and 9. Many of the product ions obtained for **18** were present for its functionally modified analogs **19−21**. But due to various modifications such as deacetylation, carbonylation, and $\Delta^{1,2}$ double bond reduction in analogs **19−21**, respectively, the mass values of the product ions in the analogs varied with respect to the product ions obtained for **18** (Scheme 2).

The highest mass product ion at m/z 407.2211 (73.04%) of **18** was generated by the neutral loss of $[M − AcOH + H]^+$ (Figure 8). The product ion at m/z 389.2106 (17.68%) of **18** was formed through the D-ring protonation followed by the neutral loss of acetoxyl and water molecule whereas the product ion at m/z 299.2001 (15.02%) of **18** was formed through the D-ring protonation following deacetoxylation (Figures 7 and 8). The fragmentation routes for the product ions at m/z 407.2211, 389.2106, and 299.2001 of **18** were evident by the presence of product ion at the same mass in analog **19**; at m/z 405.2055, 387.1949, and 297.1845 in **20**; and at m/z 409.2358, 391.2252, and 301.2150 in **21**, respectively. The mass differences observed for the analogs were associated with the C7 carbonyl functionality and the $\Delta^{1,2}$ double bond reduction, respectively.

The B-ring cleavage in the product ion at m/z 407.2211 of **18** generated the product ion at m/z 271.1325 (26.06%) of **18** (Figure 8). The product ions at m/z 259.1326 (10.74%) and 257.1169 (16.59%) of **18** were formed through the D-ring protonation following cleavage of the A- and B-rings (Figure 9). The initiation of protonation at the furan ring of **18** followed by rearrangement led to the formation of product ion at m/z 243.1377 (9.30%) (Figure 9). The product ion at m/z 241.1584 (9.52%) of **18** was formed through the D-ring protonation followed by cleavages (Figure 7). For the product ion at m/z 213.1272 (16.54%) two different structures with the same elemental compositions were formed, i.e., **213a** and **213b**, generated through the D-ring protonation and furan ring protonation, both followed by rearrangements, respectively (Figures 8 and 9). The product ions at m/z 199.1117 (11.75%) and 187.1117 (9.58%) of **18** were formed through furan ring protonation followed by deacetoxylation and rearrangements (Figure 8). The product ion at m/z 163.1117 (14.70%) of **18** was formed through the D-ring protonation followed by deacetoxylation (Figure 8). The protonation initiated at the furan ring gives rise to product ions at m/z 161.0961 (16.22%) and 137.0961 (20.14%) of **18** (Figures 8 and 9). The product ion at m/z 137.0961 of **18** was also formed through the D-ring protonation following cleavages (Figure 8). The cleavage at the B-ring in the product ion at m/z 407.2211 of **18** led to the formation of low mass product ion at m/z 121.1014 (13.0%) (Figure 8). The D-ring protonation and subsequent cleavages led to the formation of product ion at m/z 109.0287 (69.85%) of **18** (Figure 8). The D-ring protonation generated the product ions at m/z 107.0859 (10.90%) and 81.0340 (14.89%) of **18** containing a B-ring and a furan ring, respectively (Figure 7). The fragmentation routes for the product ions at m/z 271.1325, 259.1326, 257.1169, 243.1377, 241.1584, 213.1272 (**213a**, **213b**), 199.1117, 187.1117, 175.1117 (**175a**), 163.1117, 161.0961, 135.0805 (**135a**), 121.1014, 109.0287, 107.0859, and 81.0340 appeared at the same mass in all analogs (**19−21**), thereby supporting the proposed fragmentation pathway.

The cleavage of epoxide moiety from the product ion at m/z 299.2001 of **18** formed the product ion at m/z 269.1896 (14.45%) (Figure 8). For the product ion at m/z 175.1117 (15.22%) of **18** two different structures with the same elemental compositions were formed, i.e., **175a** and **175b**, both generated through the D-ring protonation following cleavages (Figures 7 and 9). The A-ring protonation followed by cleavage at the B-ring formed the product ion at m/z 149.0961 (100%) of **18** (Figure 9). For the product ion at m/z 135.0805 (40.30%) two different structures with the same elemental compositions were formed, i.e., **135a** and **135b** (Figure 7). The product ion at m/z 135.0805 (**135a**) was formed through the D-ring protonation following cleavages in the C/D-rings and contained a furan moiety, whereas the product ion at m/z 135.0805 (**135b**) was formed through the D-ring protonation followed by neutral loss of an acetoxyl moiety, a retro-Diels−Alder mechanism, and a 1,3 shift. The fragmentation routes for the product ions at m/z 269.1896, 175.1117 (**175b**), 149.0961, 137.0961, and 135.0805 (**135b**) appeared at the same mass in analogs **19** and **20** and at m/z 271.2047, 177.1270, 151.1114, 139.1114, and 137.0958, respectively, in the $\Delta^{1,2}$ double bond reduced analog **21**. The structure and mechanism of formation of the product ions at m/z 213.1272 (**213a**), 175.1117, 149.0961, 137.0961, 135.0805 (**135a**, **135b**), 121.1014, and 109.0287 originating from the precursor ion of **18** occur by a similar mechanism as discussed for the product ions of **2**.
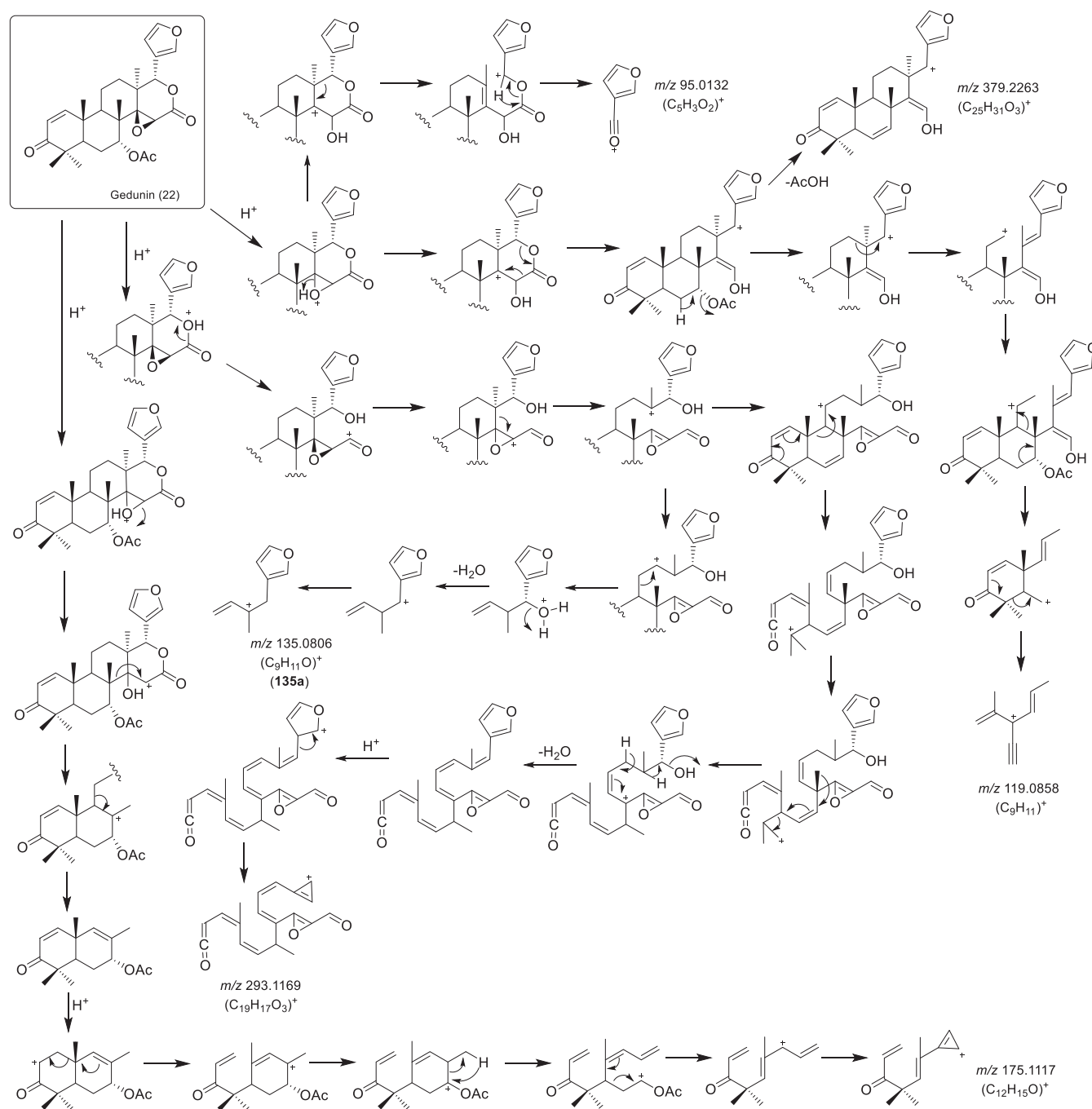
Figure 10. Tentative fragmentation pattern obtained from the product ion scan of the precursor ion of gedunin at m/z 483.2379.

2.5.3. MS/MS Characterization of Gedunin (22) and Its Derivatives. The tentative fragmentation pattern obtained by the HCD-MS/MS of the precursor ion of gedunin (**22**) having a precursor ion of $[M + H]^+$ at m/z 483.2379 was subjected to MS/MS studies in 25% NCE, which generated product ions at m/z 95.0132, 119.0858, 135.0806, 137.0962, 149.0962, 161.0597, 175.0754, 175.1117, 253.1585, 267.1377, 293.1169, 379.2263, and 423.2161 (Table 3), is represented in Figures 10 and 11. The product ions obtained for **22** were also observed in its functionally modified analogs **23**–**31** either at the same mass values or at corresponding mass values. A total of seven semisynthesized derivatives, **23** (7-deacetylgedunin), **24** (7-oxogedunin), **25** (1,2-dihydrogedunin), **26** (1,2-α-epoxygedunin), **27** (1,2-α-epoxy-7-deacetylgedunin), **28** (1,2-dihydro-3β-

hydroxygedunin), and **29** [(1,3-^{2}H)-1,2-dihydro-3β-hydroxygedunin] and two biotransformed derivatives **30** (11β-hydroxygedunin)[41,42] and **31** (12β-hydroxygedunin), were used for elucidation of the fragmentation pathway for **22**. The C7 deacetylation of **22** yielded the analog **23**, and further oxidation of **23** at C7 yielded the analog **24**. The reduction of the $\Delta^{1,2}$ double bond in **22** formed analog **25**. The A-ring epoxidation of **22** formed analog **26** which was deacetylated at C7 to yield analog **27**. The reduction at the C3 carbonyl and the $\Delta^{1,2}$ double bond in **22** formed analog **28**. The derivative **29** is the isotopolog of **28**. The C11 and C12 hydroxylation of **22** formed analogs **30** and **31**, respectively (Scheme 3).

The higher mass product ion at m/z 423.2161 (34.74%) of **22** was formed by the neutral loss of $[M − AcOH + H]^+$ (Figure 11)
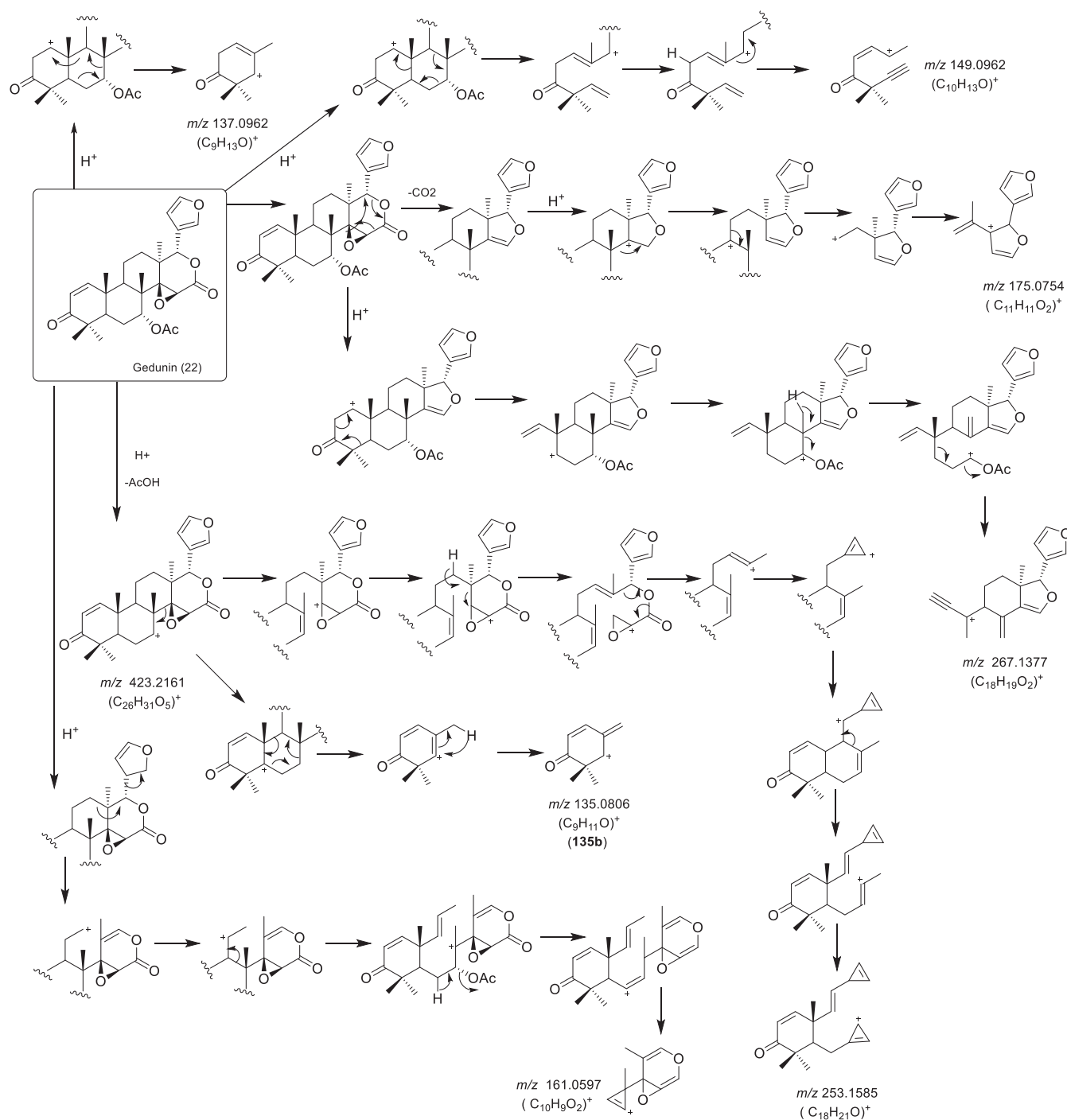
Figure 11. Tentative fragmentation pattern obtained from the product ion scan of the precursor ion of gedunin at m/z 483.2379.

as observed with azadiradione as well as epoxyazadiradione and their derivatives. This fragmentation route was supported by the presence of product ion at the same mass in analog **23**; at m/z 421.1999 in **24**; at m/z 425.2313 in **25**; at m/z 439.2110 in **26** and **27**; at m/z 427.2461 in **28**; and at m/z 421.2007 in **30** and **31**. The mass differences observed in the analogs were associated with the B-ring dehydroxylation, the reduction at the $\Delta^{1,2}$ double bond/conjugated carbonyl moiety, the A-ring epoxidation, and the C-ring dehydration. This fragmentation pathway was evident by the presence of product ion with increased mass at m/z 429.2588 in isotopolog **29**. The product ion at m/z 379.2263 (15.04%) of **22** was formed by the neutral loss of [M −

AcOH − CO_2 + H]$^+$ (Figure 10). This fragmentation pathway was favored by the presence of the product ion at the same mass in analog **23**; at m/z 395.2208 in **24**, **26**, and **27**; at m/z 381.2415 in **25**; at m/z 383.2568 in **28**; and at 377.2114 in **30** and **31**. The mass differences observed in the analogs were associated with the C7 carbonyl, the A-ring epoxidation, the reduction at the $\Delta^{1,2}$ double bond/conjugated carbonyl moiety, and the C-ring dehydration. This fragmentation pathway was confirmed by the presence of product ion with increased mass at m/z 385.2692 in isotopolog **29**. The product ion at m/z 293.1169 (16.56%) of **28** was formed through the D-ring protonation followed by rearrangement and cleavages (Figure
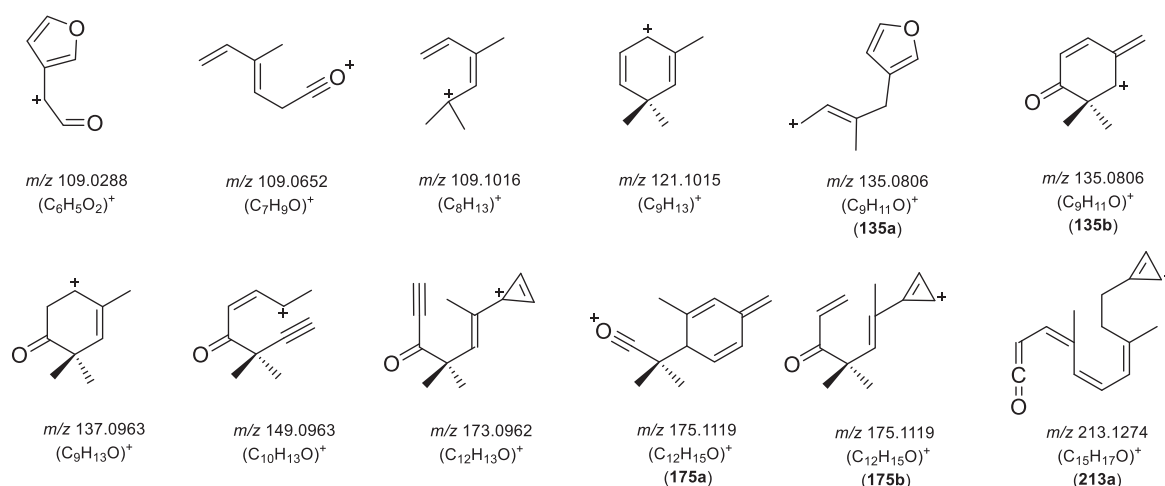
Figure 12. Key MS/MS fragments observed in basic limonoids.

10). This fragmentation route was supported by the presence of product ions at the same mass in analogs **23−27**, **30**, and **31** and at m/z 297.1472 in **28** which was due to the reduced $\Delta^{1,2}$ double bond and C3 carbonyl. This fragmentation route was further confirmed by the presence of product ion with increased mass at m/z 299.1597 in isotopolog **29**. The rearrangement at the D-ring followed by the A-ring protonation formed the product ion at m/z 267.1377 (31.34%) of **22** (Figure 11). This fragmentation route was favored by the presence of product ions at the same mass in analogs **23−27**; at m/z 269.1527 in **28**, and m/z 265.1241 in **30** and **31**. The mass differences observed in the analogs were associated with the reduction of the conjugated carbonyl moiety and the C-ring dehydration, respectively. This fragmentation route was evident by the presence of the product ion with increased mass at m/z 270.1586 in isotopolog **29**. The cleavage at the C-ring in the product ion at m/z 423.2161 of **22** formed another product ion at m/z 253.1585 (10.93%) containing A- and B-rings (Figure 11). This fragmentation pathway was supported by the presence of product ions at the same mass in analogs **23**, **24**, **30**, and **31**; m/z 255.1737 in **25**; at m/z 269.1533 in **26** and **27**; and at m/z 257.1890 in **28**. The mass differences observed in the analogs were due to the reduction at the $\Delta^{1,2}$ double bond/C3 carbonyl and the A-ring epoxidation. This fragmentation pathway was validated by the presence of product ion with increased mass at m/z 259.2017 in isotopolog **29**. The initiation of protonation at the D-ring followed by cleavages yielded the product ion at m/z 175.1117 (5.09%) of **22** (Figure 10). This fragmentation pathway was favored by the presence of product ions at the same mass in analogs **23**, **24**, **26**, **27**, **30**, and **31**; at m/z 177.1270 in **25** and at m/z 161.1325 **28**. The mass difference observed in the analogs was associated with the reduction in the $\Delta^{1,2}$ double bond/C3 carbonyl. Further, this fragmentation pathway was verified by the presence of product ion with increased mass at m/z 163.1446 in isotopolog **29**. The product ion at m/z 175.0754 (13.56%) of **22** was formed by the neutral loss of CO_2 from the D-ring followed by protonation and this fragmentation pathway was supported by the presence of product ions at the same mass in all analogs **23−31** (Figure 11). The protonation initiated at the furan ring followed by the C-ring cleavage formed the product ion at m/z 161.0597 (49.07%) of **22**, and this fragmentation pathway was favored by the presence of product ions at the same mass in all analogs **23−31** (Figure 11). The product ions at m/z 149.0962 (16.84%) and 137.0962 (100%)

of **22** were formed through the A-ring protonation followed by the B-ring cleavage (Figure 11). These fragmentation pathways for the product ion at m/z 149.0962 and 137.0962 of **22** were favored by the presence of product ions at the same mass in analogs **23**, **24**, **26**, **27**, **30**, and **31**; at m/z 151.1114 and 139.1115 in **25**; and at m/z 135.1165 and 123.1167 in **28**, respectively. The mass differences observed in the analogs were associated with the reduction in the $\Delta^{1,2}$ double bond/C3 carbonyl. Further, the fragmentation pathways were evident by the presence of product ion with increased mass at m/z 137.1292 and 125.1294 in isotopolog **29** corresponding to product ions at m/z 149.0962 and 137.0962 of **22**, respectively. For the product ion at m/z 135.0806 (44.07%) of **22**, two different structures (**135a**, **135b**) with the same elemental compositions were formed (Figures 10 and 11). The protonation initiated at the D-ring followed by the cleavage generated the product ion at m/z 135.0806 (**135a**) of **22** which contained intact furan ring. This fragmentation route was supported by the presence of product ions at the same mass in analogs **23−29** and varied at m/z 133.0650 in **30**, **31** due to the C-ring dehydration. The retro-Diels−Alder reaction in the product ion at m/z 423.2161 of **22** generated the product ion at m/z 135.0806 (**135b**). This fragmentation pathway was favored by the presence of product ions at the same mass in analogs **23**, **24**, **26**, **27**, **30**, and **31**; at m/z 137.0958 in **25**; and at m/z 139.1115 in **28**. The mass differences observed in the analogs were associated with the reduced $\Delta^{1,2}$ double bond/C3 carbonyl. Further, the fragmentation route was confirmed by the presence of product ion with increased mass at m/z 141.123 in isotopolog **29**. The product ion at m/z 119.0858 (13.05%) of **22** was formed through protonation initiated at the D-ring followed by rearrangement (Figure 10). This fragmentation route was favored by the presence of product ions at the same mass in analogs **23**, **24**, **26**, and **27**; at m/z 121.1014 in **25** and **28**; and at m/z 135.0806 in **30** and **31**. The mass differences observed in the analogs were associated with the reduced $\Delta^{1,2}$ double bond and the C11/C12 hydroxylation. Further, this fragmentation route was validated by the presence of the product ion with increased mass at m/z 122.1075 in isotopolog **29**. The product ion at m/z 95.0132 of **22** was formed through protonation initiated at the D-ring following cleavage (Figure 10). The product ions at m/z 95.0132, 161.0597, and 175.0754 of **22** are the signature product ions for the gedunin type skeleton. The structure and mechanism of formation of product
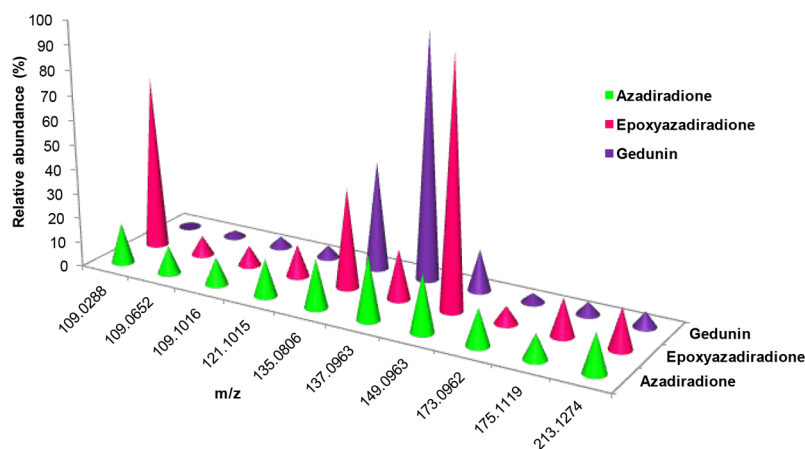
Figure 13. Key Mass fragments of basic limonoid and their abundance in azadiradione, epoxyazadiradione, and gedunin.

ions at m/z 135.0806 (**135b**) 137.0962, and 149.0962 originating from the precursor ion of **22** occurs by similar mechanism as discussed for product ions of **2**.

2.6. Key MS/MS Fragments for Identification of Basic Limonoids. The basic limonoids azadiradione (**2**) (m/z 451.2479), epoxyazadiradione (**18**) (m/z 467.2428), and gedunin (**22**) (m/z 483.2377) are formed from azadirone (**1**) (m/z 437.2686). Here, we discuss in detail the key MS/MS fragments appearing in all basic limonoids which serves as signature fragments to identify the basic limonoid skeleton in plant crude extracts (Figure 12). Both the product ions at m/z 109.0288 and 135.0806 (**135a**) contained intact furan rings generated by protonation initiated at the D-ring. The product ion at m/z 109.0652 was generated by protonation initiated at the A-ring and contained cleaved portions of A- and B-rings. The product ion at m/z 137.0963 contained an intact A-ring derived by protonation which further underwent rearrangement giving rise to two product ions at m/z 109.1016 and 121.1015. The formation of product ion at m/z 135.0806 (**135b**) was initiated by protonation and subsequent elimination of the C7 acetoxyl group and fragment containing an intact A-ring. The protonation initiated at the D-ring led to the formation of product ion at m/z 149.0963 containing an A-ring. The product ions at m/z 173.0962 and 175.1119 (**175b**) were formed by the protonation initiated at the D-ring following cleavage at the B-ring. However, the product ion at m/z 175.1119 (**175a**), which was also formed by protonation initiated at the D-ring, contained an intact B-ring and cleaved portions of the A-ring. The product ion at m/z 213.1274 (**213a**) was generated by the D-ring protonation and contained cleaved portions of A-, B-, and C-rings.

The key mass fragments of basic limonoid were generated for all three limonoids, viz., **2**, **18**, **22**, with varying abundance levels (Figure 13). The lowest common product ion at m/z 109.0288 ($C_6H_5O_2$, 16.40%) of **2** appeared in **18** with an abundance of 69.85% and was completely absent in **22**. The next low mass product ion at m/z 109.0652 (C_7H_9O, 11.05%) of **2** appeared in **18** and **22** with abundances of 7.78 and 2.57%, respectively. The abundances of another product ion at m/z 109.1016 (C_8H_{13}, 11.13%) in **2** were only 8.14 and 4.32% abundant in **18** and **22**, respectively. The product ion at m/z at 121.1015 (C_9H_{13}, 14.98%) of **2** was 13.0 and 4.88% abundant in **18** and **22**, respectively. Another common product ion at m/z 135.0806 ($C_9H_{11}O$) consisted of two different structures (**135a**, **135b**) with the same elemental compositions in all three basic

limonoids. The product ion at m/z 135.0806 (**135a**) contained the intact furan ring, and that at m/z 135.0806 (**135b**) contained an intact A-ring. The abundances of this product ion were 19.72, 40.30, and 44.07% in **2**, **18**, and **22**, respectively. The abundance of product ion at m/z 137.0963 ($C_9H_{13}O$) was 100% in **22** but it was 25.80 and 20.14% in **2** and **18**, respectively.

The abundances of common product ion at m/z 149.0963 ($C_{10}H_{13}O$) were 100, 23.37, and 16.84% in **18**, **2**, and **22**, respectively. The abundances of product ion at m/z 173.0962 ($C_{12}H_{13}O$, 14.90%) in **2** were reduced to half in **18** (7.01%) and one-fourth in **22** (3.70%). The abundances of product ion at m/z 175.1119 ($C_{12}H_{15}O$, 5.09%) in **22** were two times higher in **2** (10.17%) and three times high in **18** (15.22%). The abundances of highest mass product ion at m/z 213.1274 ($C_{15}H_{17}O$) were 15.98, 16.54, and 6.14% in **2**, **18**, and **22**, respectively. These characteristic product ions are key fragments in identifying and characterizing the basic limonoid structure with highest accuracy using UHPLC−MS/MS in plant crude extracts.

3. CONCLUSION

In conclusion we have synthesized different analogs of basic limonoids, i.e., azadiradione, epoxyazadiradione, and gedunin isolated from Neem. Among the synthesized derivatives eight analogs were novel. We have developed the most reliable, accurate, and easily reproducible UHPLC−MS/MS based method for analysis of SFRs, based on structural modifications. To further confirm the proposed fragmentation pathways, we synthesized isotopologs and subjected them to MS/MS fragmentation. The comparative analysis of MS/MS fragments of basic limonoids and their isotopologs led to the identification of the origin of product ions, which aided in establishing the fragmentation pathway. Our investigation on SFRs generated the fragment library for three basic limonoids which can be utilized for high-throughput screening in identification of similar skeletons (tetranortriterpenoids) in crude extracts of plants with highest accuracy. Also it can be utilized for qualitative and quantitative analysis of these molecules involved in metabolism or biosynthesis and degradation. We identified both low and high mass fragments specific to the basic limonoid skeleton and traced their origin. The appearances of high mass product ions were specific for each basic limonoid and hence acted as signature ions.

4. EXPERIMENTAL SECTION

4.1. Materials and Solvents. Neem fruits were collected from the CSIR-NCL campus in Pune, India. The methodology of isolation of Neem limonoids is discussed in detail in the Supporting Information. LC—MS grade solvents were purchased from Merck. Technical grade solvents were distilled prior to use. Chemicals and reagents required for synthesis were procured from Merck. Milli-Q water was used for LC—MS experiments. Thin layer chromatography was done using silica gel-G coated plates "TLC Silica gel 60 F254" Merck. Silica gel for column chromatography was procured from Merck.

4.2. Instrumentation. UHPLC-ESI-MS/MS samples were analyzed by using Q-Exactive Orbitrap coupled with Accela 1250 pump (Thermo Scientific). 1D (1H, 13C, DEPT-135) and 2D (COSY, NOESY, HSQC, HMBC) NMR spectra were recorded on a Bruker spectrophotometer (500 MHz, 400 MHz, 200 MHz) in $CDCl_3$, acetone-d_6, and methanol-d_4, and the TMS peak or residual solvent peak was assigned as the reference.

4.3. UHPLC—MS and MS/MS Conditions. A Waters Acquity BEH C18 UPLC column (2.1 mm × 100 mm) having 1.7 μm particle size was used to run the samples of concentration 0.2 mg/mL in methanol. Five microliters of sample was injected using a 90% methanol/water isocratic solvent program (10 min.) with 300 μL/min flow rate. Water used in the solvent system contained 0.1% formic acid. The following tune method parameters were used: sheath gas (nitrogen) flow rate 45 units; auxiliary gas (nitrogen) flow rate 10 units; sweep gas (nitrogen) flow rate 2 units; spray voltage 3.60 |kV|; spray current 3.70 μA; capillary temperature 320 °C; s-lens RF level 50 and heater temperature 350 °C. MS and MS/MS experiments were performed on a Data Dependent Acquisition mode (parallel reaction monitoring) within the mass range of m/z 100−1000 in the positive ion mode. Data were analyzed using Thermo scientific Xcalibur software.

ASSOCIATED CONTENT

Ⓢ Supporting Information

The Supporting Information is available free of charge at https://pubs.acs.org/doi/10.1021/acsomega.1c03697.

    Experimental procedures for extraction/isolation of limonoids and chemical synthesis of analogs along with their analytical data such as NMR and LC—MS spectra are provided (PDF)

AUTHOR INFORMATION

Corresponding Author

Hirekodathakallu V. Thulasiram − *Chemical Biology Unit, Division of Organic Chemistry, CSIR-National Chemical Laboratory, Pune 411008, India; Academy of Scientific and Innovative Research (AcSIR), Ghaziabad 201002, India; CSIR-Institute of Genomics and Integrative Biology, New Delhi 110007, India;* ◎ orcid.org/0000-0002-0108-1143; Phone: 91 20 2590 2478; Email: hv.thulasiram@ncl.res.in; Fax: 91 20 2590 2629

Authors

Fayaj A. Mulani − *Chemical Biology Unit, Division of Organic Chemistry, CSIR-National Chemical Laboratory, Pune 411008, India; Academy of Scientific and Innovative Research (AcSIR), Ghaziabad 201002, India*

Sharvani S. Nandikol − *Chemical Biology Unit, Division of Organic Chemistry, CSIR-National Chemical Laboratory,*

Pune 411008, India; Academy of Scientific and Innovative Research (AcSIR), Ghaziabad 201002, India

Saikat Haldar − *Chemical Biology Unit, Division of Organic Chemistry, CSIR-National Chemical Laboratory, Pune 411008, India*

Complete contact information is available at:
https://pubs.acs.org/10.1021/acsomega.1c03697

Author Contributions

#These authors contributed equally to this work.

Notes

The authors declare no competing financial interest.

■ REFERENCES

(1) Bouslimani, A.; Sanchez, L. M.; Garg, N.; Dorrestein, P. C. Mass Spectrometry of Natural Products: Current, Emerging and Future Technologies. *Nat. Prod. Rep.* **2014**, *31* (6), 718−729.

(2) Jarmusch, A. K.; Cooks, R. G. Emerging Capabilities of Mass Spectrometry for Natural Products. *Nat. Prod. Rep.* **2014**, *31* (6), 730−738.

(3) Krug, D.; Müller, R. Secondary Metabolomics: The Impact of Mass Spectrometry-Based Approaches on the Discovery and Characterization of Microbial Natural Products. *Nat. Prod. Rep.* **2014**, *31* (6), 768−783.

(4) Milman, B. L. General Principles of Identification by Mass Spectrometry. *TrAC, Trends Anal. Chem.* **2015**, *69*, 24−33.

(5) Smyth, W. F.; McClean, S.; Hack, C. J.; Ramachandran, V. N.; Doherty, B.; Joyce, C.; O'Donnell, F.; Smyth, T. J.; O'Kane, E.; Brooks, P. The Characterisation of Synthetic and Natural-Product Pharmaceuticals by Electrospray Ionisation-Mass Spectrometry (ESI-MS) and Liquid Chromatography (LC)-ESI-MS. *TrAC, Trends Anal. Chem.* **2006**, *25* (6), 572−582.

(6) Smyth, W. F.; Smyth, T. J. P.; Ramachandran, V. N.; O'Donnell, F.; Brooks, P. Dereplication of Phytochemicals in Plants by LC-ESI-MS and ESI-MS N. *TrAC, Trends Anal. Chem.* **2012**, *33*, 46−54.

(7) Weissberg, A.; Dagan, S. Interpretation of ESI(+)-MS-MS Spectra—Towards the Identification of "Unknowns. *Int. J. Mass Spectrom.* **2011**, *299* (2−3), 158−168.

(8) Wu, H.; Guo, J.; Chen, S.; Liu, X.; Zhou, Y.; Zhang, X.; Xu, X. Recent Developments in Qualitative and Quantitative Analysis of Phytochemical Constituents and Their Metabolites Using Liquid Chromatography—Mass Spectrometry. *J. Pharm. Biomed. Anal.* **2013**, *72* (151), 267−291.

(9) Xing, J.; Xie, C.; Lou, H. Recent Applications of Liquid Chromatography-Mass Spectrometry in Natural Products Bioanalysis. *J. Pharm. Biomed. Anal.* **2007**, *44* (2), 368−378.

(10) Demarque, D. P.; Crotti, A. E. M.; Vessecchi, R.; Lopes, J. L. C.; Lopes, N. P. Fragmentation Reactions Using Electrospray Ionization Mass Spectrometry: An Important Tool for the Structural Elucidation and Characterization of Synthetic and Natural Products. *Nat. Prod. Rep.* **2016**, *33* (3), 432−455.

(11) Murray, K. K.; Boyd, R. K.; Eberlin, M. N.; Langley, G. J.; Li, L.; Naito, Y. Definitions of Terms Relating to Mass Spectrometry (IUPAC Recommendations 2013). *Pure Appl. Chem.* **2013**, *85* (7), 1515−1609.

(12) De Rosso, M.; Tonidandel, L.; Larcher, R.; Nicolini, G.; Dalla Vedova, A.; De Marchi, F.; Gardiman, M.; Giust, M.; Flamini, R. Identification of New Flavonols in Hybrid Grapes by Combined Liquid

Chromatography-Mass Spectrometry Approaches. *Food Chem.* **2014**, *163*, 244−251.

(13) Jaiswal, R.; Kuhnert, N. Identification and Characterization of Two New Derivatives of Chlorogenic Acids in Arnica (Arnica Montana L.) Flowers by High-Performance Liquid Chromatography/Tandem Mass Spectrometry. *J. Agric. Food Chem.* **2011**, *59*, 4033−4039.

(14) Kee, C. L.; Ge, X.; Low, M. Y.; Koh, H. L. Structural Elucidation of a New Sildenafil Analogue Using High-Resolution Orbitrap Mass Spectrometry. *Rapid Commun. Mass Spectrom.* **2013**, *27* (12), 1380−1384.

(15) Marchal, A.; Génin, E.; Waffo-Téguo, P.; Bibès, A.; Da Costa, G.; Mérillon, J. M.; Dubourdieu, D. Development of an Analytical Methodology Using Fourier Transform Mass Spectrometry to Discover New Structural Analogs of Wine Natural Sweeteners. *Anal. Chim. Acta* **2015**, *853* (1), 425−434.

(16) Uchida, H.; Taira, Y.; Yasumoto, T. Structural Elucidation of Palytoxin Analogs Produced by the Dinoflagellate Ostreopsis Ovata IK2 Strain by Complementary Use of Positive and Negative Ion Liquid Chromatography/Quadrupole Time-of-Flight Mass Spectrometry. *Rapid Commun. Mass Spectrom.* **2013**, *27* (17), 1999−2008.

(17) Prakash, C.; Shaffer, C. L.; Nedderman, A. Analytical Strategies for Identifying Drug Metabolites. *Mass Spectrom. Rev.* **2007**, *26* (3), 340−369.

(18) Holčapek, M.; Kolářová, L.; Nobilis, M. High-Performance Liquid Chromatography-Tandem Mass Spectrometry in the Identification and Determination of Phase i and Phase II Drug Metabolites. *Anal. Bioanal. Chem.* **2008**, *391* (1), 59−78.

(19) Tolonen, A.; Turpeinen, M.; Pelkonen, O. Liquid Chromatography-Mass Spectrometry in in Vitro Drug Metabolite Screening. *Drug Discovery Today* **2009**, *14* (3−4), 120−133.

(20) Zhu, M.; Zhang, H.; Humphreys, W. G. Drug Metabolite Profiling and Identification by High-Resolution Mass Spectrometry. *J. Biol. Chem.* **2011**, *286* (29), 25419−25425.

(21) Allwood, J. W.; Goodacre, R. An Introduction to Liquid Chromatography-Mass Spectrometry Instrumentation Applied in Plant Metabolomic Analyses. *Phytochem. Anal.* **2010**, *21* (1), 33−47.

(22) Sumner, L. W.; Lei, Z.; Nikolau, B. J.; Saito, K. Modern Plant Metabolomics: Advanced Natural Product Gene Discoveries, Improved Technologies, and Future Prospects. *Nat. Prod. Rep.* **2015**, *32* (2), 212−229.

(23) Lei, Z.; Huhman, D. V.; Sumner, L. W. Mass Spectrometry Strategies in Metabolomics. *J. Biol. Chem.* **2011**, *286* (29), 25435−25442.

(24) Berendsen, B. J. A.; Zuidema, T.; de Jong, J.; Stolker, L. A. A. M.; Nielen, M. W. F. Discrimination of Eight Chloramphenicol Isomers by Liquid Chromatography Tandem Mass Spectrometry in Order to Investigate the Natural Occurrence of Chloramphenicol. *Anal. Chim. Acta* **2011**, *700* (1−2), 78−85.

(25) Milman, B. L. A Procedure for Decreasing Uncertainty in the Identification of Chemical Compounds Based on Their Literature Citation and Cocitation. Two Case Studies. *Anal. Chem.* **2002**, *74* (7), 1484−1492.

(26) Nagy, G.; Pohl, N. L. B. Complete Hexose Isomer Identification with Mass Spectrometry. *J. Am. Soc. Mass Spectrom.* **2015**, *26* (4), 677−685.

(27) Stow, S. M.; Crescentini, T. M.; Forsythe, J. G.; May, J. C.; McLean, J. A.; Hercules, D. M. Structural Characterization of Methylenedianiline Regioisomers by Ion Mobility-Mass Spectrometry, Tandem Mass Spectrometry, and Computational Strategies. 3. MALDI Spectra of 2-Ring Isomers. *Anal. Chem.* **2017**, *89* (18), 9900−9910.

(28) Gaudêncio, S. P.; Pereira, F. Dereplication: Racing to Speed up the Natural Products Discovery Process. *Nat. Prod. Rep.* **2015**, *32* (6), 779−810.

(29) Barrek, S.; Paisse, O.; Grenier-Loustalot, M. F. Analysis of Neem Oils by LC−MS and Degradation Kinetics of Azadirachtin-A in a Controlled Environment : Characterization of Degradation Products by HPLC−MS-MS. *Anal. Bioanal. Chem.* **2004**, *378* (3), 753−763.

(30) Calza, P.; Medana, C.; Sarro, M.; Rosato, V.; Aigotti, R.; Baiocchi, C.; Minero, C. Photocatalytic Degradation of Selected Anticancer

Drugs and Identification of Their Transformation Products in Water by Liquid Chromatography-High Resolution Mass Spectrometry. *J. Chromatogr. A* **2014**, *1362*, 135−144.

(31) García-Reyes, J. F.; Molina-Díaz, A.; Fernández-Alba, A. R. Identification of Pesticide Transformation Products in Food by Liquid Chromatography/Time-of-Flight Mass Spectrometry via "Fragmentation- Degradation" Relationships. *Anal. Chem.* **2007**, *79* (1), 307−321.

(32) Medana, C.; Calza, P.; Baiocchi, C.; Pelizzetti, E. Liquid Chromatography Tandem Mass Spectrometry as a Tool to Investigate Pesticides and Their Degradation Products. *Curr. Org. Chem.* **2005**, *9* (9), 859−873.

(33) Wu, Y. The Use of Liquid Chromatography-Mass Spectrometry for the Identification of Drug Degradation Products in Pharmaceutical Formulations. *Biomed. Chromatogr.* **2000**, *14* (6), 384−396.

(34) Vetter, W. F.; McLafferty, W.; Turecek, F. Interpretation of Mass Spectra. Fourth Edition (1993). University Science Books: Mill Valley, California; 1994; Vol. 23.

(35) Haldar, S.; Mulani, F. A.; Aarthy, T.; Dandekar, D. S.; Thulasiram, H. V. Expedient Preparative Isolation and Tandem Mass Spectrometric Characterization of C-Seco Triterpenoids from Neem Oil. *J. Chromatogr. A* **2014**, *1366*, 1−14.

(36) Aarthy, T.; Mulani, F. A.; Pandreka, A.; Kumar, A.; Nandikol, S. S.; Haldar, S.; Thulasiram, H. V. Tracing the Biosynthetic Origin of Limonoids and Their Functional Groups through Stable Isotope Labeling and Inhibition in Neem Tree (Azadirachta Indica) Cell Suspension. *BMC Plant Biol.* **2018**, *18* (1), 1−21.

(37) Champagne, D. E.; Koul, O.; Isman, M. B.; Scudder, G. G. E. E.; Neil Towers, G. H. Biological Activity of Limonoids from the Rutales. *Phytochemistry* **1992**, *31* (2), 377−394.

(38) Haldar, S.; Phapale, P. B.; Kolet, S. P.; Thulasiram, H. V. Expedient Preparative Isolation, Quantification and Characterization of Limonoids from Neem Fruits. *Anal. Methods* **2013**, *5* (20), 5386−5391.

(39) Crotti, A. E.; Fonseca, T.; Hong, H.; Staunton, J.; Galembeck, S. E.; Lopes, N. P.; Gates, P. J. The Fragmentation Mechanism of Five-Membered Lactones by Electrospray Ionisation Tandem Mass Spectrometry. *Int. J. Mass Spectrom.* **2004**, *232* (3), 271−276.

(40) Crotti, A. E. M.; Lopes, J. L. C.; Lopes, N. P. Triple Quadrupole Tandem Mass Spectrometry of Sesquiterpene Lactones: A Study of Goyazensolide and Its Congeners. *J. Mass Spectrom.* **2005**, *40* (8), 1030−1034.

(41) Haldar, S.; Mulani, F. A.; Aarthy, T.; Thulasiram, H. V. Whole-Cell Mediated 11β-Hydroxylation on the Basic Limonoid Skeleton by Cunninghamella Echinulata. *J. Org. Chem.* **2015**, *80* (12), 6490−6495.

(42) Haldar, S.; Kolet, S. P.; Thulasiram, H. V. Biocatalysis: Fungi Mediated Novel and Selective 12β- or 17β-Hydroxylation on the Basic Limonoid Skeleton. *Green Chem.* **2013**, *15* (5), 1311.